JAIST Repository
https://dspace.jaist.ac.jp/

Title	Near-Capacity-Achieving Design of BICM-ID Based IDMA
Author(s)	ORMSUB, Soulisak
Citation	
Issue Date	2012-03
Type	Thesis or Dissertation
Text version	author
URL	http://hdl.handle.net/10119/10422
Rights	
Description	Supervisor:松本　正，情報科学研究科，修士

JAIST
JAPAN
ADVANCED INSTITUTE OF
SCIENCE AND TECHNOLOGY

Japan Advanced Institute of Science and Technology

Near-Capacity-Achieving Design of BICM-ID Based IDMA

By Soulisak Ormsub

A thesis submitted to
School of Information Science,
Japan Advanced Institute of Science and Technology,
in partial fulfillment of the requirements
for the degree of
Master of Information Science
Graduate Program in Information Science

Written under the supervision of
Professor Tad Matsumoto

March, 2012

Near-Capacity-Achieving Design of BICM-ID Based IDMA

By Soulisak Ormsub (1010015)

A thesis submitted to
School of Information Science,
Japan Advanced Institute of Science and Technology,
in partial fulfillment of the requirements
for the degree of
Master of Information Science
Graduate Program in Information Science

Written under the supervision of
Professor Tad Matsumoto

and approved by
Professor Tad Matsumoto
Professor Mineo Kaneko
Associate Professor Kiyofumi Tanaka

February, 2012 (Submitted)

Copyright © 2012 by Soulisak Ormsub

I certify that I have prepared this Master's Thesis by myself without any inadmissible outside help.

Soulisak Ormsub
JAIST, Feb, 06, 2012

Author : _____

Date : _____

Supervisor : _____

Acknowledgments

I attended Japan Advanced Institute of Science and Technology (JAIST) since April 2010 for further studying on the field of information science. My research work under the supervision of Prof. Tad Matsumoto was full of fun and meaningful discussion. With his friendly attitude, invaluable supervision, great enthusiasm and encouragement, my life and study can be smoothly and successfully passed with great lessons and achievements. I would like to express my deepest gratitude to this incredible person. He is really one of the best professors on this planet.

I am also appreciative of the friendship and help from Matsumoto lab's members, especially, the guidance and support from Assistant Prof. Khoirul Anwar.

I am sincerely grateful to the financial support provided by Hitachi Kokusai Electric Inc. as well as their invaluable advices from the industry's viewpoint.

Finally, I would like to take this opportunity to provide my deepest thanks to my parents, as well as brothers and sisters, who have never stopped supporting and encouraging me every single moment of my life.

Soulisak Ormsub
JAIST Japan, Feb, 2012.

Abstract

Bit-Interleaved Coded Modulation with Iterative Detections/Decoding (BICM-ID) is considered one of the most promising candidates for future wireless communication transmission scheme, since it can achieve high spectral efficiency and diversity gain over the AWGN as well as frequency-flat Rayleigh fading channels. Recently, Kisho Fukawa, a graduate from JAIST in March 2011, proposed an EXIT-constrained BICM-ID system, which uses simple single parity check and irregular repetition codes, combined with partial accumulator and unbalanced Extended Mapping (EM). The Bit Error Rate (BER) performance shows that, with this approach, the BER threshold only around 0.54 dB away from the Shannon limit can be achieved. However, due to the DC-Offset problem, the BICM-ID with unbalanced mapping may not be practical for the real systems.

This thesis, first of all, introduces a Modulation Doping technique to solve the unbalanced mapping problem based on the same system model as that used in the unbalanced mapping case. It is found that, with the proposed doping technique, even with balanced labelling pattern the performance is as good as the one obtained by unbalanced labellings case. This thesis further investigates the performance of the BICM-ID with higher order modulation such as 16-QAM EM. The results show that with the higher spectrum efficiency, the signal-noise-ratio (SNR) threshold at only roughly 0.4 dB and 0.2 dB away from the Shannon and 16-QAM coding limit can be achieved, respectively, with the proposed technique. Finally, since it is known that the very good performances can be achieve with the proposed simple BICM-ID, this thesis applies the designed BICM-ID to Interleave Division Multiple Access (IDMA), which is considered a bandwidth efficient multiple access scheme for the future generation of wireless communication systems.

Keywords: BICM-ID, single parity check code, irregular repetition code, extended mapping, unbalanced mapping, balanced mapping, modulation doping technique, higher order modulation, 16-QAM, IDMA.

Contents

Achievements

Conference papers:

- S. Ormsub, K. Fukawa, K. Anwar, A. Tolli, Tad. Matsumoto, "Near-Capacity-Achieving Simple BICM-ID", presented in IEEE CTW2011, Sitges, Catalonia, Spain, Jun 20th-22nd, 2011, (Poster presentation).

Journal papers:

- S. Ormsub, K.Fukawa, K. Anwar, Tad. Matsumoto, "Simple BICM-ID with Higher Order Modulation Extended Mapping", Submitted to IEEE Communications Letters, 2011.
- K. Fukawa, S. Ormsub, K. Anwar, A. Tolli, Tad. Matsumoto, "EXIT-constrained BICM-ID Design Using Extended Mapping", accepted for publication in EURASIP, 2012.
- S. Ormsub, K. Anwar, Tad. Matsumoto, "A Very Low Complexity Coded BICM-ID based IDMA", to be submitted to IEEE Transaction Information Theory, 2012.

List of Figures

List of Tables

Chapter 1

Introduction

Mobile wireless communication, in the last few decades, was an expensive communication medium, and therefore, only a few selected individuals of people and/or organizations could take benefits from it. Now, it has grown so rapidly and become ubiquitous communication tool that are commonly used by people all around the world. It started with analogue mobile radio systems in 1980s, known as the first generation or 1G, followed by 2G, the first digital mobile systems, then 3G, the first broadband multi-media mobile communication systems, and presently 4G evolution scenario-making is one of the hottest topics of discussion in the world. The basic concepts of our next mobile communication systems are to realize high data rate transmission, low latency, and low energy consumption. Many researchers have been devoted to developing such technology that can satisfy exponentially increasing high demands for a variety of services.

Shannon was the person who first derived the theoretical limits, known as Shannon limit, of data transmission in 1948 [1]. He showed that information can only be transmitted without any errors or arbitrarily low Bit Error Rate (BER) if the rate of channel coding is smaller than the so-called channel capacity. In other words, for the reliable transmission, the channel capacity must be larger than the data transmission rate. Therefore, approaching channel capacity or Shannon limit based on powerful channel coding schemes are required to enable high data rate transmission with efficient energy use. Because high order modulation can transmit several bits per symbol with a given signal point, it has been widely used to improve the bandwidth and power efficiency. However, since the complexity grows when the order of modulation increases, there is still a limit of using the very high order modulation, e.g. 256-QAM, 512-QAM.

It has been recognized that the joint design of coding and modulation can optimize the performance of the wired and wireless transmission systems. One of the well-known schemes based on this idea is Bit-Interleaved Coded Modulation with Iterative Detection/Decoding (BICM-ID). It is comprised of a serial concatenation of channel encoder, interleaver, and mapper at the transmitter. Iterative detection and decoding, following the turbo principle [2], is performed at the receiver side. It is found that the iterative demapping-and-decoding plays very important role in improving the performance of the system, where demapper and decoder exchange their *extrinsic* Log Likelihood Ratio (LLR) via interleaver and deinterleaver, respectively. According to the area property of

the serially concatenated system, BICM-ID performance analysis can rely on the matching of the Extrinsic Information Transfer (EXIT) curves [3] of the demapper and decoder. Several researches have been devoted to finding the design of the suitable coding scheme as well as the optimal symbol mapping, e.g. Quadratic Assignment Problem (QAP) [5], Reactive Tabu Search (RTS) [6], Binary Switching Algorithm (BSA) [7], which can be seen simply as determining the mapping rule from binary vectors to complex constellation points.

Recently, Kisho Fukawa, a graduate from JAIST in March 2011, proposed an EXIT-constrained BICM-ID system, which uses simple single parity check and irregular repetition codes, combined with partial accumulator and unbalanced Extended Mapping (EM). He proposed an EXIT-constraint Binary Switching Algorithm (EBSA), which is simply seen as combining Linear Programming (LP) technique together with BSA, to design the optimal labeling mapping rule and the node degree distribution for the system. With this approach, it is guaranteed that very narrow convergence tunnel in the EXIT chart opens until the demapper and decoder curves reach closely (1.0, 1.0) point of the Mutual Information (MI), yielding a close Shannon limit threshold signal-noise-ratio (SNR), and no error floor. The BER performance shows that the threshold SNR of only roughly 0.54 dB away from the Shannon limit can be achieved. However, due to the DC-Offset problem, the BICM-ID with unbalanced mapping may not be practical for the real systems. The main reason that he used unbalanced EM instead of balanced EM is because of good matching between the demapper and decoder curves without crossing each other in the early point of MI. While this can not be avoided when the balanced EM is used; the crossing point of the two curves happen at the (0.0, 0.0) point of MI, and therefore, the LLR exchange does not start, yielding the system unworkable.

This thesis, first of all, introduce a Modulation Doping (MD) technique to solve the unbalanced mapping problem based on the same system model as that used in the unbalanced mapping case. It is found that, with this technique, even with balanced labeling mapping patterns the performance is as good as the one obtained by using unbalanced mapping scheme. This thesis further investigates the performance of the BICM-ID with higher order modulation. The results show that, to achieve a spectrum efficiency of 1.33 bits per 16-QAM symbol, the SNR threshold at only roughly 0.4 dB and 0.2 dB away from the Shannon and 16-QAM coding limit can be achieved, respectively, with the proposed technique. Finally, based on the key findings that the very good performances can be achieve with the proposed simple BICM-ID, this thesis applies the designed BICM-ID to Interleave Division Multiple Access (IDMA), which is considered a bandwidth efficient multiple access scheme for forth generation wireless communication systems. It is shown through simulation that the proposed BICM-ID based IDMA with Multiple User Detection (MUD) technique outperforms conventional IDMA systems, while the computational complexity is still very low.

This thesis is organized as follows: in **Chapter 2**, as the tools for analysis and evaluating the system, the fundamental knowledge about EXIT and BER curves are clearly stated. Then, in **Chapter 3**, the system model for low and high order modulations are presented. Moreover, the basic theories as well as the mathematical basic of the technique

used in this thesis are introduced in this chapter. **Chapter 4** shows the system models of the IDMA for both Single User Detection (SUD) and MUD cases. In addition, each detection technique as well as their roles in the system diagram will be explained. **Chapter 5** presents the results of simulation conducted to evaluate the performance of techniques described in **Chapter 3** and **Chapter 4**. Both EXIT Analysis and BER performance results will be shown in this chapter. Finally, the conclusions will be drawn, and the technique left as future studying will be discussed in **Chapter 6**.

Chapter 2

System Evaluation Tools

As the tools for evaluating performances of the proposed systems in this thesis, EXIT charts and Monte Carlo simulation are adopted. The basic principle of EXIT chart, the demapper and decoder EXIT curves, and the analyzing technique are expressed in **Section 1**. The fundamental of Monte Carlo simulation for the evaluation of BER of the iterative schemes is stated in **Section 2**.

2.1 EXIT Chart Analysis

The fundamental understanding of EXIT curve is provided in the form of several theorems in this section. It covers the ways how to analyse the communication systems, how to optimize the outer code, and how to control the convergence behavior of iterative process at a certain SNR. For the purpose of analysis, design, and optimization of concatenated systems based on turbo principle, the EXIT chart was first proposed by ten Brink [3]. The demapping-and-decoding trajectory in the EXIT chart shows the real exchange of *extrinsic* information between them, and helps predicting the position where turbo-cliff happens as well as BER after the certain iterations.

2.1.1 Relationship Between the Entropy and Mutual Information

To understand what MI is, it is necessary, first of all, to know what the entropy indicates. In the information theory, the entropy was first defined by Claude E. Shannon [1]. It is the measure of uncertainty of a message or random variable. In other words, it indicates, under a certain constraint, what the best possible lossless compression is in communications. It is expressed as:

$$H(M) = -\sum_{m \in M} P(m) \log_2 P(m), \tag{2.1}$$

where $H(M)$ represents the entropy of information symbol m, which is included in information sequence M. $P(\cdot)$ indicates the appearance probability of source symbol. The

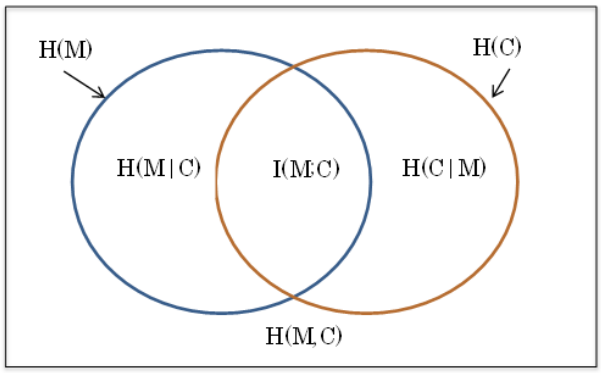

Figure 2.1: Relationship between Entropy and MI diagram

conditional entropy can be further described as:

$$H(M|C) = \sum_{m,c} P(m,c) \log \frac{P(c)}{P(m,c)}, \tag{2.2}$$

where C is the known information sequence, and $P(m,c)$ returns the probability that C=c and M=m. The quantity of mutual dependence of M and C expresses the MI between M and C, $I(M;C)$, as:

$$\begin{aligned}
I(M;C) &= \sum_{m,c} P(m,c) \log \frac{P(m,c)}{P(m) \cdot P(c)} && (2.3)\\
&= \sum_{m,c} P(m,c) \log \frac{P(m|c)}{P(m)} && (2.4)\\
&= -\sum_{m,c} P(m,c) \log P(m) + \sum_{m,c} P(m,c) \log P(m|c) && (2.5)\\
&= -\sum_{m} P(m) \log P(m) + \sum_{m,c} P(m,c) \log P(m|c) && (2.6)\\
&= H(M) - H(M|C) && (2.7)\\
&= I(C;M) && (2.8)\\
&= H(C) - H(C|M) && (2.9)\\
&= H(M) + H(C) - H(M,C), && (2.10)
\end{aligned}$$

where M and C are the two discrete information sequences or random variables. In summary, the relationship between entropy and MI is depicted in Fig. 2.1.

2.1.2 Output Mutual Information of Inner Code and Outer code

The output MIs of the demapper (inner code) and decoder (outer code) in the BICM-ID system can be calculated by using coded bits and LLRs values output from demapper and

decoder, respectively. LLRs output from demapper is generated based on the received signal and *extrinsic* information from the channel decoder, while the LLRs output from decoder is calculated using the *extrinsic* information from the demapper. Since interleaver helps the output LLRs from demapper and decoder uncorrelated to each other; the *extrinsic* LLR is approximated by the Gaussian random variable as the number of iterations increases, and by assuming the known transmitted information bit x suffered from zero mean Gaussian noise with variance σ_n^2, the LLRs can be expressed as:

$$L = \vartheta_l x + n_l \tag{2.11}$$

with

$$\vartheta_l = \frac{2}{\sigma_n^2}, \tag{2.12}$$

$$\sigma_l^2 = \frac{4}{\sigma_n^2}, \tag{2.13}$$

where ϑ_l and σ_l indicate the mean of LLR and variance of Gaussian distributed equivalent noise n_l, respectively. Since LLR is the continuous random value, based on the equation (2.3), MI calculation can be remodeled as:

$$I(B;L) = \frac{1}{2}\sum_{b\in 0,1}\int_{-\infty}^{+\infty} P(l|b)\cdot \log_2 \frac{2\cdot P(l|b)}{P(l|b=0)+P(l|b=1)} dl, \tag{2.14}$$

with

$$P(l,b) = P(l|b)P(b), \tag{2.15}$$

$$P(b=0) = P(b=1) = \frac{1}{2}, \tag{2.16}$$

$$P(l) = \frac{1}{2}(P(l|b=0)+P(l|b=1)), \tag{2.17}$$

where $(b,l) \in (B,L)$. B and L are the coded bits and its corresponding LLRs, respectively. In order to avoid calculating integration, symmetry and consistency of $P(l|b)$ are assumed as:

$$P(l|b=0) = P(-l|b=1), \tag{2.18}$$

$$P(l|b=0) = P(-l|b=1)\cdot e^l. \tag{2.19}$$

and thus,

$$P(l|b=0) = P(l|b=1)\cdot e^l, \tag{2.20}$$

Invoking the ergodicity of LLR, computing the MI can be replaced by time-averaging. In reality, this assumption is not always satisfied in many communication schemes. Nevertheless, it has been found that with the consistency assumption, accurate and reliable MI

calculation is still possible [4]. Therefore, the equation (2.14) can be approximated as:

$$\begin{aligned} I(B;L) &= 1 - \int_{-\infty}^{+\infty} P(l|b=0) \cdot \log_2(1+e^{-l}) dl && (2.21) \\ &= 1 - E[\log_2(1+e^{-l})|b=0] && (2.22) \\ &\approx 1 - \frac{1}{Q}\sum_{q=1}^{Q} \log_2(1+e^{-\hat{b}_q l_q}),\ with\ \hat{b} = 1-2b, && (2.23) \end{aligned}$$

where equation (2.23) is reasonable under the assumption that the sampling number Q is large enough and ergodic [4]. For the rest of this thesis, equation (2.23) is used to compute the MIs of demapper and decoder.

2.1.3 J-Function based Mutual Information

In [4], it is shown that MI can be expressed by so called J function. The J function connects the MI and variance of LLRs following the Gaussian approximation distribution as:

$$J(\sigma) = I(\sigma_l = \sigma). \tag{2.24}$$

If we further assume binary Gaussian channel, equation (2.24) can be approximated as:

$$J(\sigma) = (1 - 2^{H_1 \sigma^{2H_2}})^{H_3}, \quad where \quad \begin{cases} H_1 = 0.3073 \\ H_2 = 0.8935 \\ H_3 = 1.1064 \end{cases} \tag{2.25}$$

and

$$J^{-1}(I) = (-\frac{1}{H_1}\log_2(1 - I^{\frac{1}{H_3}}))^{\frac{1}{2H_2}}. \tag{2.26}$$

The $J(\sigma)$ and $J^{-1}(I)$ functions in equations (2.25) and (2.26) convert the square-root variance σ of LLR to MI, and its inverse, respectively. By using these functions, it is convenient to measure the output MI and LLR of the inner and outer codes. In addition, if the variance is known, the BER of the system can be obtained through the error function which will be derived in the next section.

2.1.4 An Example of EXIT Chart Analysis

An exemplifying EXIT chart is shown in Fig. 2.2. There are two curves in this chart; the demapper and decoder curves. The demapper curve indicates the output *extrinsic* MI of demapper, while the decoder curve shows the *extrinsic* MI of decoder itself. Both of them use the output via interleaver/deinterleaver of the other side as the *a priori* information. Therefore, the X-axis can be denoted as the *a priori* and *extrinsic* MI for the demapper and decoder, respectively, while Y-axis gives the inversion of this. The

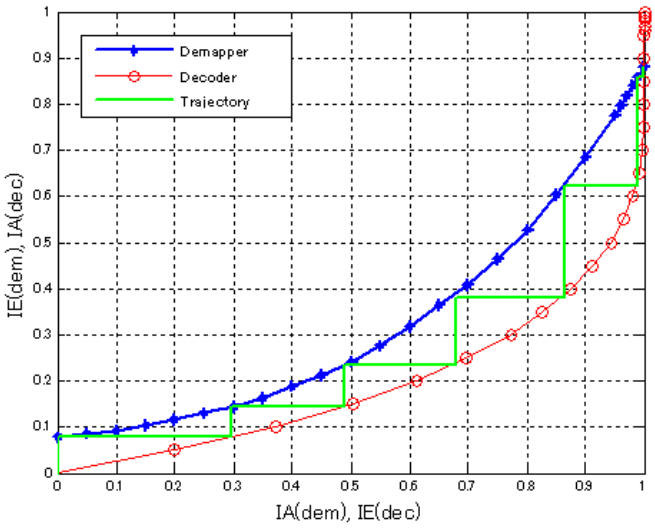

Figure 2.2: EXIT Chart

step-wise line between the demapper and decoder curves is called trajectory. It tells us the convergence behaviour through real information exchange between the demapper and decoder. It should be noted that, for the successful transmission, according to Shannon's channel coding theorem [1], the demapper EXIT curve must always be allocated above the decoder EXIT curve while keeping the tunnel between two curves opening.

In the EXIT chart, illustrated in Fig. 2.2, there are three properties related to the area can be noticed. The first one is the area under the decoder EXIT curve corresponding to the coding rate R of the system which can be written as:

$$R = \frac{b_{in}}{b_{out}}, \tag{2.27}$$

where b_{in} and b_{out} indicate the number of input and output information bits of channel encoder, respectively. The second is the area under the demapper curve which is equivalent to the constellation constraint capacity (CCC). Since the labeling rule for mapping at a certain SNR does not cause any significant effects on CCC, the area under the demapper EXIT curve still remains the same when the labelling mapping rule, for the same modulation format, is changed. The last is corresponding to the area between demapper and decoder EXIT curves: it indicates how efficient the transmission scheme is; it is preferable to design a code so that the area under the demapper and decoder EXIT curves are almost exactly the same, which indicates that there is no information loss due to the mismatch, resulting in the performance very close to the Shannon limit. However, in reality, it is difficult to design such a code, and therefore, the rate loss still remains in many cases in the designed systems. In fact, reducing the rate loss, which is also a goal of this thesis, has been the major research target in wireless communication community since Shannon's landmark paper in 1948.

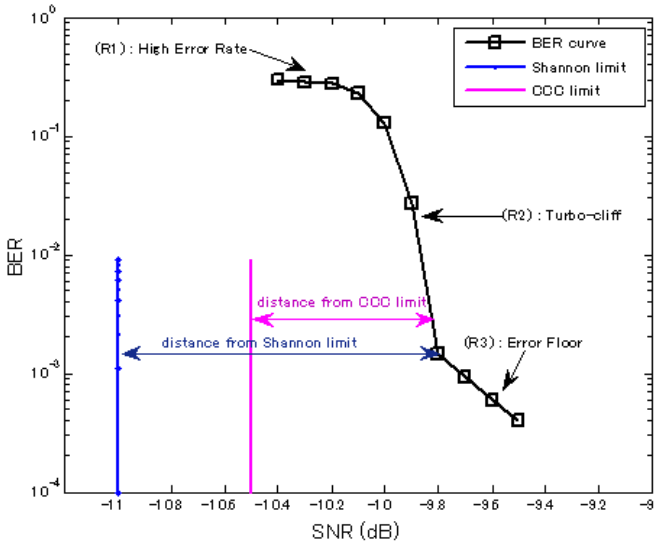

Figure 2.3: Bit Error Rate Chart

2.2 BER Chart Analysis

For the iterative transmission systems, the BER performance curve exhibits major comprise of three regions, as depicted in Fig. 2.3. The region *R1* indicates that no gain can be obtained via the iterative processing of the inner code (demapper) and the outer code (decoder). This means that the *extrinsic* information exchange between the inner and outer codes has no impact in reducing BER. The problem can be solved only when the SNR is increased. In the region *R2*, sudden reduction in BER is observed due to a slight increase in SNR, which is a result of the convergence via several iterations of information exchange between two components at the receiver. In addition, according to the intersection point of MI of the inner and outer codes on the EXIT curve, it determines how sharp BER decrease, so-called turbo-cliff, can be achieved; the deeper the cliff, the lower error rate, promising good BER performance. In the region *R3*, the error floor appears. The error floor occurs mainly due to the intersection point of the two EXIT curves is not at (1.0, 1.0) point of MI. This problem can be solved by applying partial accumulator that pushes up the right most part of the inner code to the very close (1.0, 1.0) point of MI.

The BER of the system can be obtained by using the error function if the variance σ of decoder's soft output *a posteriori* LLR is known. It can be derived as:

$$P_{BER} = \frac{1}{2} erfc(\frac{\sigma}{2\sqrt{2}}). \tag{2.28}$$

From the observations of the properties of iterative scheme's BER charts, in order to achieve as good performance as possible, it is mandatory to design a system with negligible error floor. Blue curve shows the Shannon limit or capacity limit, supported by Shannon's

channel coding theorem, and the gap between the limit and the threshold SNR where the turbo-cliff happens corresponding to the rate loss, which is due to the mismatch in convergence properties between the inner and outer codes. Assuming Gaussian codebook, the Shannon limit can be calculated by:

$$SNR_{Shannon\ limit} = 2^{\eta} - 1, \tag{2.29}$$

where η denotes the spectrum efficiency or capacity of the system. Red curve is the Constellation Constraint Capacity (CCC) limit of inner code, which is computed as:

$$SNR_{CCC\ limit} = 2^{C_a} - 1, \tag{2.30}$$

where

$$C_a = \underbrace{\max}_{P(k)} \sum_{k \in K} \int_{-\infty}^{+\infty} P(r,k) \log_2 \frac{P(k,r)}{P(k)P(r)} dr \tag{2.31}$$

with

$$\begin{aligned} P(r) &= \sum_{k=1}^{M_d} P(r,k) && (2.32) \\ &= \sum_{k=1}^{M_d} \left(\frac{1}{M_d} \right) \cdot \left(\frac{e^{-\frac{|r-s_k|^2}{2\sigma^2}}}{\sqrt{2\pi\sigma^2}} \right), && (2.33) \\ P(k) &= \int_{-\infty}^{+\infty} P(r,k) dr = \frac{1}{M_d}, && (2.34) \end{aligned}$$

and

$$P(r,k) = \left(\frac{e^{-\frac{|r-s_k|^2}{2\sigma^2}}}{\sqrt{2\pi\sigma^2}} \right) \cdot \left(\frac{1}{M_d} \right), \tag{2.35}$$

where continuous distribution $P(r)$ indicates the appearance probability of received signal r under zero mean, and variance σ^2 identically independently distributed (i.i.d) Gaussian noise. $P(k)$ is the independent discrete *apriori* probability of the k^{th} transmitted symbol, while $P(k,r)$ denotes the joint distribution probability. M_d and s_k indicate the number of signal points and the k^{th} discrete signal point in the constellation diagram. Throughout this thesis, 2^{M_l}-quadrature amplitude modulation ($2^{M_l} - QAM$) is assumed.

Chapter 3

BICM-ID for Low and High Order Modulation

In this chapter, first of all, the principle of BICM-ID and its merits are introduced. Then, the proposed BICM-ID system model is depicted. The roles of each part in the system model will be simply explained as the basic understanding of the system, After that. This chapter also covers explanatory sections of channel encoder, interleaver, accumulator, 2^M-QAM, demapper, BCJR decoding, and channel decoder. Finally, the complexity of the system is investigated for both demapping and decoding processes.

3.1 BICM-ID Principle

Bit-Interleaved Coded Modulation with Iterative Detections/Decoding (BICM-ID) is considered one of the most promising candidates for future wireless communication transmission scheme, since it can achieve high spectral efficiency in AWGN, as well as diversity gain in frequency-flat Rayleigh fading channels. The general structure of conventional BICM-ID is shown Fig. 3.1. It comprises of a serial concatenation of channel encoder, interleaver, and mapper at the transmitter. Iterative detection and decoding, following the turbo principle [2], is performed at the receiver side. It is found that the iterative demapping-and-decoding plays very important role in improving the performance of the system, where the demapper and decoder exchange the *extrinsic* LLR via interleaver and deinterleaver, respectively.

In the BICM-ID system, interleaver and deinterleaver, expressed later in detail, are sandwiched between channel encoder and mapper, demapper and channel decoder, respectively. Since this thesis assumes block fading, the interleaver[1] is used to to make the *a priori* LLR statistically independent, while the *extrinsic* LLR between them being exchanged. In the iterative process, the ratio of the probabilities of bits $P(+1)$ and $P(-1)$, known as LLR, defined in the next section, updated by the demapper/decoder are fed

[1]Conventionally, interleaver has been used to randomize the burst errors caused by some practical impairments and/or fading channels. However, the purpose of using the interleaver in the turbo codes or turbo systems is to randomize the code itself according to Shannon's channel coding theorem.

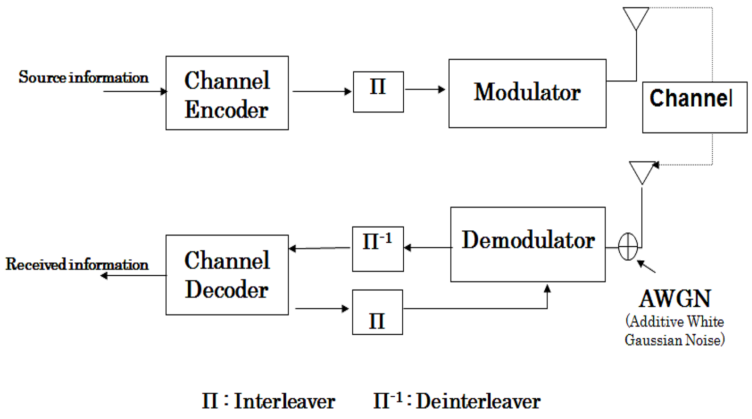

Figure 3.1: Conventional BICM-ID

back to the decoder/demapper as *a priori* information. This process is called *turbo loop* (or turbo iteration), and will be repeated until it converges or no more gain in mutual information can be obtained by the iterations. The decoder makes the final decision based on the *a posteriori* LLR (L_p), defined by:

$$L_p = L_a + L_e, \tag{3.1}$$

where L_a and L_e are the *a priori* and *extrinsic* LLRs, respectively.

3.2 Design of BICM-ID for 4-QAM and 16-QAM

In this section, first of all, the proposed system model and the roles of each part will be described in detail. Then, the design of labelling rule for mapping, both for 4-QAM and 16-QAM, and channel coding's degree distribution, are presented. The proposed system model for both 4-QAM and 16-QAM is generalized in Fig. 3.2. It is composed of a serial concatenation of channel encoder, interleaver, accumulator, and mapper at the transmitter. For channel coding, the simple single parity check code (SPCC) and irregular repetition code (IRC) are used. Accumulator (ACC), described in the later section, is added to allow the demapper EXIT curve to reach a point close enough to MI (1.0, 1.0) point. For the mapper, EM is adopted. However, if there exists that the two components EXIT curves intersected each other at a point not close enough to the MI (1.0, 1.0) point, by using not suitable labelling rule, the MD technique has to be used. MD can be seen as combining more than one labelling rules together in order to push up/down the left most part of the demapper EXIT curve. At the receiver side, iterative detection and decoding, following the turbo principle [2], is performed. However, since the accumulator is introduced, the BCJR decoding [9] is also involved in the decoding process.

Note that the system model described above was originally proposed by Kisho Fukawa in his master thesis in 2011, where he used unbalanced labelling pattern. This thesis

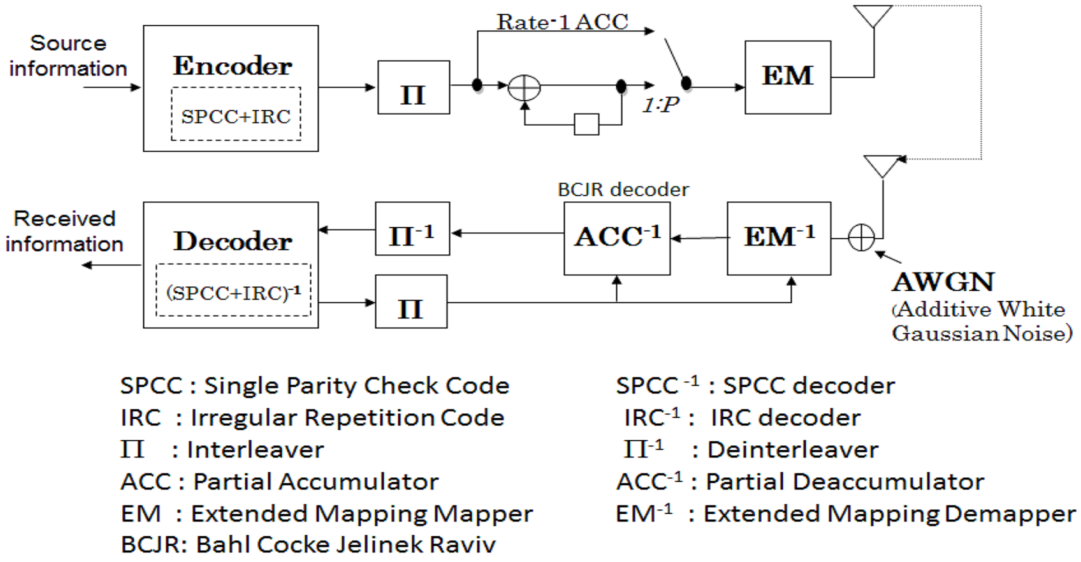

Figure 3.2: Proposed BICM-ID

further investigates the performance of this system assuming 4-QAM and 16-QAM with balanced labelling rule. Therefore, the only dissimilarity from Kisho Fukawa's case is that the different modulations, modulation doping, and higher modulation, e.g. 16-QAM, are used in the mapper.

3.2.1 Channel Coding

The source information, assumed to take binary form, in general, is sent to the destination or receiver by the transmission scheme through communication channels. One of the channels that plays very important role in reducing the negative effects of errors, caused by the noisy channel during the transmission using limited spectrum is channel encoding. It adds some redundancy when transmitting source information. According to the Shannon's channel coding theorem, the length of transmitted information sequence $N^{'}$ can be described as:

$$N^{'} = N + Rd, \tag{3.2}$$

where N and Rd are the length of source information sequence and redundancy, respectively. The coding rate R for the system is defined as:

$$R = \frac{N}{N'}. \tag{3.3}$$

It may be observed from the equations (3.2) and (3.3) that the more redundancy are added, the more reliable transmission can be achieved. However, it is the outcome of the

use of extra-bandwidth at the same time. Therefore, when the redundancy addition is adopted for error protection, the transmission chain design should be aiming at achieving the closed Shannon limit BER performance, in order to maximize the power efficiency of the system.

In Fig. 3.2, as a channel coding, it uses SPCC and IRC. This means that the source information bit sequence is encoded by SPCC and IRC in succession. SPCC is used to add a single parity bit to every $(d_c - 1)^{th}$ information bits in the source sequence, while IRC is then employed to repeat the bits sequence, after adding parity check, according to the irregular variable node degree distribution $d_{v,i}$. Note that d_c here is defined as the check node degree. Fig. 3.3 gives an example of this encoding process. In this example, $d_c = 5$, the variable note degrees $d_{v,i}$ and their ratios α_i are $\{d_{v,i}, \alpha_i\} = \{(3, 4), (0.2, 0.8)\}$. Parity bit addition is performed by appending 0 or 1 to the end of every $(d_c - 1)^{th}$ bits, depending on the number of binary 1s existing in the bits sequence. If the number of 1s is even, then 0 is added. Otherwise, 1 will be appended. The repetition process satisfying the specified irregular degree allocations then follows the IRC encoding process. In the example described above, the first 20 percent of bits sequence are repeated by 3 times, while the remainders are duplicated 4 times. After the entire portion of the source information is SPCC-and-IRC encoded, the sequence is then input to an interleaver and passed into the mapper. The spectrum efficiency $\eta_{SPCCIRC}$ of the proposed coded modulation scheme can be calculated as:

$$\eta_{SPCCIRC} = l_{map} \cdot R_{SPCCIRC} \tag{3.4}$$

bits per symbol, with the code rate of this coding scheme being

$$R_{SPCCIRC} = \frac{d_c - 1}{d_c \cdot \sum_i \alpha_i \cdot d_{v,i}}, \tag{3.5}$$

where l_{map} is the number of mapped bits per symbol. $R_{SPCCIRC}$ indicates the total coding rate of the system.

3.2.1.1 Design of Channel Coding

Determining the variable node degree distribution $d_{v,i}$ and their ratio α_i can be performed in two ways. One is by trial-and-error or empirically, and the other more systematic way is by using LP technique. The empirical way is performed by setting some node degree distribution based on experience, and after that predicts the performance by using, for example, EXIT analysis. Since the parameters obtained by this technique do not guarantee their optimality, there is a limit in achieving a good matching between the demapper and decoder EXIT curves. Therefore, the gap between two curves are still remaining, resulting far distance from the Shannon limit. The other preferable way is to use the LP technique, which guarantees the optimality of the degree distribution, so that an excellent matching between the demapper and decoder curves can be obtained, given a target spectrum efficiency.

As mentioned above that the use of LP technique is aiming at achieving near-capacity performance, and thus, maximizing the coding rate is the target of designing the proposed

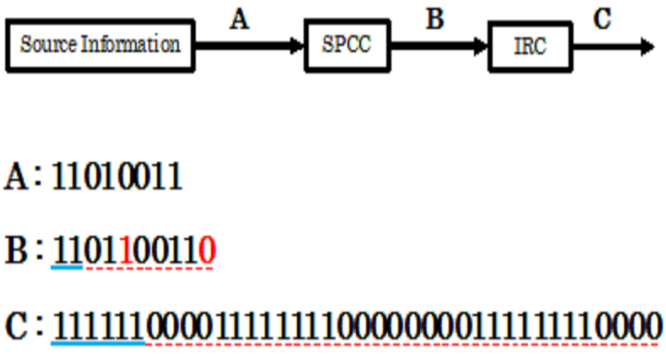

Figure 3.3: SPCC-IRC Encoding process

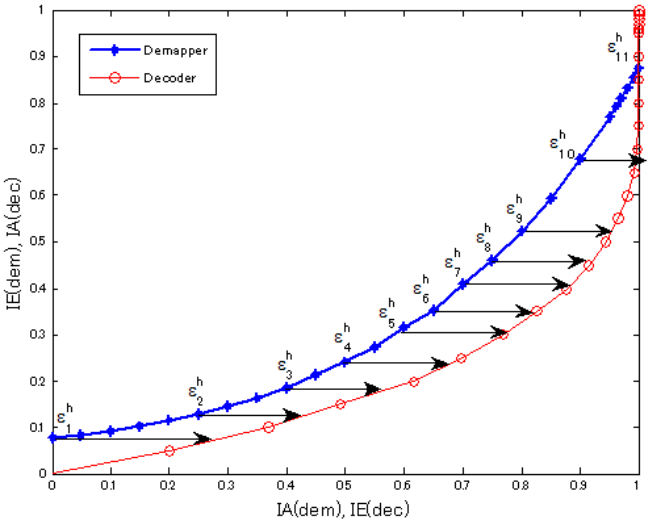

Figure 3.4: ϵ^h Settings on EXIT curve

Table 3.1: Example of Before and After Optimizing Degree Distribution

Before	$d_{v,i}$	1	2	3	4	5	6	7	8	9	10	11
	α_i	0.1	0.1	0.1	0.1	0.1	0.1	0.1	0.1	0.1	0.1	0.1
	ϵ_h	0	0	0	0	0.001	0.001	0.001	0.001	0	0	0
After	$d_{v,i}$	1	2	3	4	5	6	7	8	9	10	11
	α_i	0	0.820	0.101	0	0	0	0	0	0	0.079	0

channel coding. However, according to Shannon's channel coding theorem [1], since the successive transmission can only be achieved if the demapper EXIT curve stays above the decoder EXIT curve, while keeping the tunnel between two curves opening, the maximum code rate still has to be less than or equal to the channel capacity. In some occasions, even though over some portions of the tunnel between the two EXIT curves are opening, they intersect at some other points, and the intersection may happen at not high enough MI point. Therefore, this matter should be taken into account when determining the degree distribution of the SPCC-IRC code. Consequently, designing irregular degree allocations using the LP technique is subjected to the following constraints:

- Maximize the coding rate to be as high as possible. i.e.,

$$R_{SPCCIRC} = \max\{\frac{d_c - 1}{d_c \cdot \sum_i \alpha_i \cdot d_{v,i}}\}. \tag{3.6}$$

- Avoid the intersection between demapper and decoder EXIT curves over entire value range of MI $\in [0.0, 1.0)$ while aiming to minimize the desirable convergence tunnel.

Then, the criteria for LP can be summarized as finding α_i for each $d_{v,i}$ such that

$$\begin{aligned} &Minimize \ \sum_i \alpha_i \cdot d_{v,i}, \\ &Subject\ to \ \begin{cases} \sum_i \alpha_i = 1 \\ I_{e,dec} > I_{a,dec}, \end{cases} \end{aligned} \tag{3.7}$$

where $I_{a,dec}$ and $I_{e,dec}$ are the *a priori* and *extrinsic* MI of the decoder, respectively. Note that d_c in equation (3.6) is assumed to be constant in the LP-based optimization. To guarantee the opening of the convergence tunnel over the entire portions of MI $\in [0.0, 1.0)$, this thesis introduce a horizontal gap parameter ϵ_d^h with d being the constant index. Equation (3.7) then can be rewritten as:

$$\begin{aligned} &Minimize \ \sum_i \alpha_i \cdot d_{v,i}, \\ &Subject\ to \ \begin{cases} \sum_i \alpha_i = 1 \\ I_{e,dec,d} - I_{a,dec,d} \geq \epsilon_d^h \geq 0, \quad (for\ 0 \leq d \leq D'), \end{cases} \end{aligned} \tag{3.8}$$

where

$$I_{e,dec,d} = \frac{\sum_i \alpha_i \cdot d_{v,i} \cdot J(\sqrt{(d_{v,i} - 1) \cdot J^{-1}(I_{a,dec,d})^2 + J^{-1}(I_{e,ckn,d})^2})}{\sum_i \alpha_i \cdot d_{v,i}}. \tag{3.9}$$

However, since $I_{a,dec,d} = I_{e,dem,d}$, by replacing $I_{a,dec,d}$ with $I_{e,dem,d}$ in equation (3.9) and substituting them into equation (3.8), the criteria can be re-summarized as:

$$\begin{aligned} &Minimize \ \sum_i \alpha_i \cdot d_{v,i}, \\ &Subject\ to \ \begin{cases} \sum_i \alpha_i = 1 \\ \sum_i \alpha_i \cdot d_{v,i} \cdot (J(\sqrt{(d_{v,i} - 1) \cdot J^{-1}(I_{e,dem,d})^2 + J^{-1}(I_{e,ckn,d})^2}) + I_{a,dem,d} + \epsilon_d^h) \leq 0, \end{cases} \end{aligned} \tag{3.10}$$

Table 3.2: Irregular Degree Distribution Searching Algorithm

Algorithm 1 Irregular Degree Distribution Searcher

Initialize the $d_{v,i}$ and α_i values.
  for d_c= 2 **to** 100 **do**
    Perform Simplex algorithm based LP to obtain optimal d_c and α_i values
    Calculate the code rate $R_{SPCCIRC}$ based on d_c and α_i values
  end for
Select the optimal parameters of d_c and α_i that maximize the $R_{SPCCIRC}$

with

$$I_{e,ckn,d} = 1 - J(\sqrt{d_c - 1} \cdot J^{-1}(1 - J(\sqrt{d_v \cdot J^{-1}(I_{e,dem,d})^2}))). \tag{3.11}$$

The Table. 3.2 summarizes the LP based optimal degree allocation algorithm, where the Simplex algorithm is used for the LP. Note that the maximum value of d_c here is set as 100, but it can take any values bigger than 1 ($d_c \geq 2$). In Fig. 3.4 illustrates the idea of setting ϵ_d^h on EXIT chart. In this case, it is set according to the *a priori* MI points of demapper. An example of variable node degree distribution obtained by LP is given in Table. 3.1.

3.2.2 Design of Interleaver

Interleaver was originally introduced to help enhancing the performance of error correction in the wireless communication by making permutation of the source information sequence. It randomizes the burst errors, in general, caused by the fast fading channel, so that the error probability of a certain bit can be independent of the error probability of the neighbouring bits[1]. Therefore, the design of interleaver length is very crucial and should not be less than the number of transmitted coded bits sequence to fully randomize the burst errors. Note that the interleaved bits, if necessary, can be reordered into the original position by performing the inverse permutation of interleaving (so-called deinterleaving). Since this thesis assumes block fading, interleaver and deinterleaver does not play any roles in spreading burst error due to fast fading but keeping information exchange between inner and outer codes statistically independent in the iterative decoding process.

Fig. 3.5 gives an example of using interleaving technique. It can be observed that interleaving has a big advantage over the data transmission in current digital communication systems. Due to the effective shuffling of bits sequence, the data can be mostly recovered even the burst error happened with the help of forward error correction. On the other hand, the demerit of using interleaving is that it causes a transmission latency. This happens because of the assumption that entire block of transmitted information must be received before decoding.

There are several types of interleaver used for error correction coding, e.g. rectangular or uniform interleaver, convolutional interleaver, and random interleaver. This thesis always

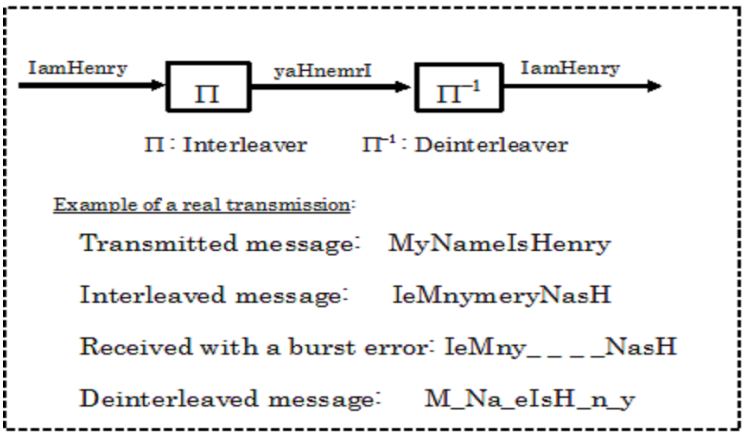

Figure 3.5: Interleaving Technique

assumes random interleaver for the entire investigations because of the reason described above.

3.2.3 Partial Accumulator

Partial accumulator (ACC) is a technique used to remove the error floor, as indicated in **Chapter 2**, from the BER performance. It was first introduced by [10] which used the memory-1 rate-1 recursive systematic convolutional codes. It was found that by using this technique, the right most part of the inner code EXIT curve can be pushed up to reach a point close enough to the (1.0, 1.0) MI point. This means that a lower error rate is achievable, compared to the case without ACC, since the higher MI is reachable and error floor can be eliminated. The partial ACC punctures the interleaved bits at every P^{th} bit to generate the accumulated bits sequence. Fig. 3.6 shows the process of this technique, which can be mathematically expressed as:

$$b_a(k) = \begin{cases} b(k), & if\ k\ mod\ P \neq 0 \\ b^{'}(k), & if\ k\ mod\ P = 0 \end{cases} \tag{3.12}$$

with

$$b^{'}(k) = b^{'}(k-1) \oplus b(k), \tag{3.13}$$

where b and b_a indicate the original input bit and the accumulated bit output from partial accumulator, respectively. $b^{'}$ denotes the bit after taking exclusive OR between itself and the original input bit. Note that the initial value $b^{'}$ is preset as zero at the first time.

3.2.4 Quadrature Amplitude Modulation (QAM)

QAM has been widely used in digital wireless communication systems. Digital systems transmit at least two binary symbol (= bit) sequence, where the polarity of the symbol,

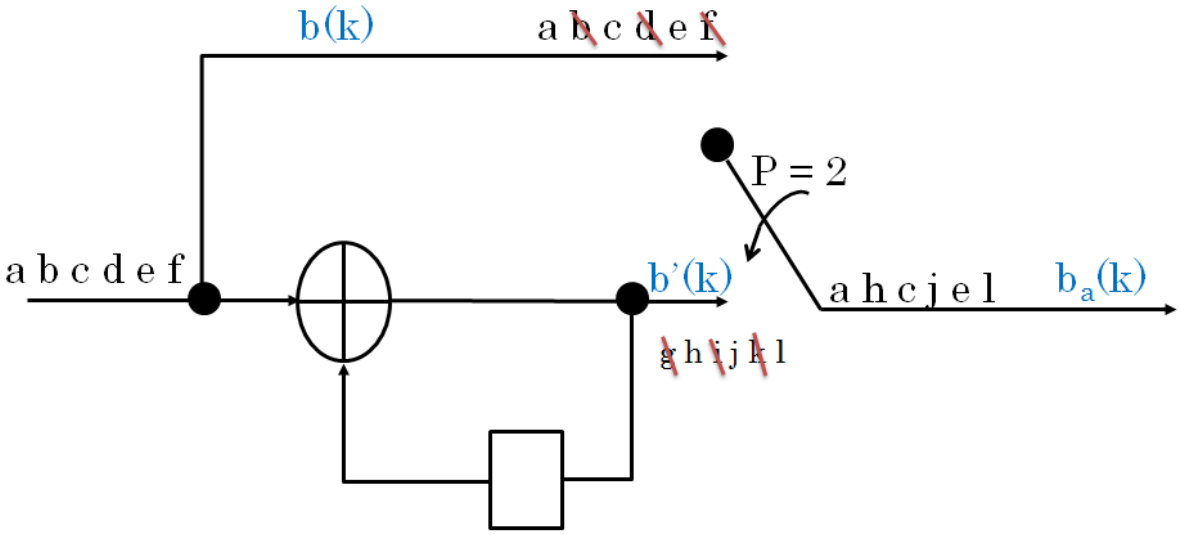

Figure 3.6: Partial Accumulator

represented by the phase being 0 or π, indicates the binary information 0 and 1, respectively. The phase may take 0, $\frac{\pi}{2}$, π, $\frac{3\pi}{2}$, which results in quadrature phase shift keying (QPSK). Together with the phase-difference, amplitude can also represents the information. The combined signal, composed of two amplitude shift keying (ASK) signals on real and imaginary axes is referred as quadrature amplitude modulation (QAM). In summary, QAM can be seen as a single carrier signal having two ASK; one is in the real domain and the other in the imaginary domain, resulting in the complex constellation point.

There are normally two kinds of QAM; rectangular QAM and non-rectangular QAM. Even though the non-rectangular QAM is expected to have a lower error rate performance than the rectangular QAM, as it imposes a practical difficulty in implementation; modulating and demodulating the rectangular QAM, especially square QAM, is most preferable for the real systems, such as 4-QAM, 16-QAM, 64-QAM, and 256-QAM. Therefore, this thesis also assumes this square constellations QAM for the investigations. Various forms of QAM are used when the higher spectrum efficiency than Binary Phase Shift Keying (BPSK) are required.

In this thesis, either 4-QAM or 16-QAM is assumed as the constellation diagram for the mapper. However, in the case that the demapper EXIT curve at a target point is extremely low or intersects with the decoder EXIT curve at a low MI point, a combined use of different mapping rules, e.g. Gray-mapping and extended mapping, may provide a good solution.

3.2.4.1 4-QAM vs. 16-QAM

The advantage of 16-QAM over 4-QAM is considered to be that it can carry more bits of source information per symbol at a time. This means that the data rate of a link

can be gradually increased according to the increase in modulation. It results in much faster data transmission with a higher level of spectrum efficiency. However, there is also a disadvantage of 16-QAM based transmission schemes; they have less resistance to interferences, fading, and noise, compared to the lower order modulation. Therefore, in many practical communication systems, the dynamic adaptive modulation technique is adopted. It aims to achieve the highest data rate, given the certain conditions of the channel. It adapts the modulations, e.g. 4-QAM and 16-QAM, based on the channel conditions.

3.2.4.2 Standard Mapping vs. Extended Mapping

The main difference between standard mapping (SM) and extended mapping (EM), as depicted in Fig. 3.7, is that the number of bits per symbol in SM is extended by $E^{'}$ bits in EM. Therefore, the total length of bits per symbol in EM can be expressed as:

$$l_{map} = l_{SM} + E^{'} \tag{3.14}$$

with

$$l_{SM} = \log_2 M_d, \tag{3.15}$$

where l_{SM} denotes the length of bits per symbol of SM, while M_d is the complex signal points for a certain constellation diagram. The other difference is that EM has an advantage of noise resistance over the SM based schemes with the same length of bits per symbol. Fig. 3.8 gives an example of 4-QAM and 16-QAM having $l_{map} = 4$ in the AWGN channel. A demerit of EM is that the ambiguity increases for demapping process due to the addition of bits per symbol. However, with the help of *a priori* information providing by the outer code, this problem can be easily solved in the iterative transmission schemes. Since there are many possible combinations between signal constellation points, the EM is considered to be a flexible way to design a code based on a certain range of SNR. Nevertheless, the design of EM is similar to SM of which the Euclidean distance spectrum ought to be optimized with full *a priori* information. Therefore, the BSA is useful when designing labelling patterns of EM.

3.2.4.3 Modulation Doping Technique

In this thesis, modulation doping (MD) technique is applied to use in the mapper for modulating the transmitted bit sequence into symbols, if the demapper EXIT curve intersects the decoder EXIT curve at a very low or (0.0, 0.0) MI point. The MD technique was first introduced in [11], referred to as irregular modulation scheme. MD technique can be seen as a way of combining different signal constellations or mapping rules on one length N code block. This thesis mixes EM with SM to lift up the left most part of the demapper EXIT curve. Since the EXIT curve of demapper with SM, including Gray and non-Gray mappings, has always bigger MI at the starting point, when *a priori* MI equals zero, than the case with EM, the left most part of demapper can be adapted flexibly after

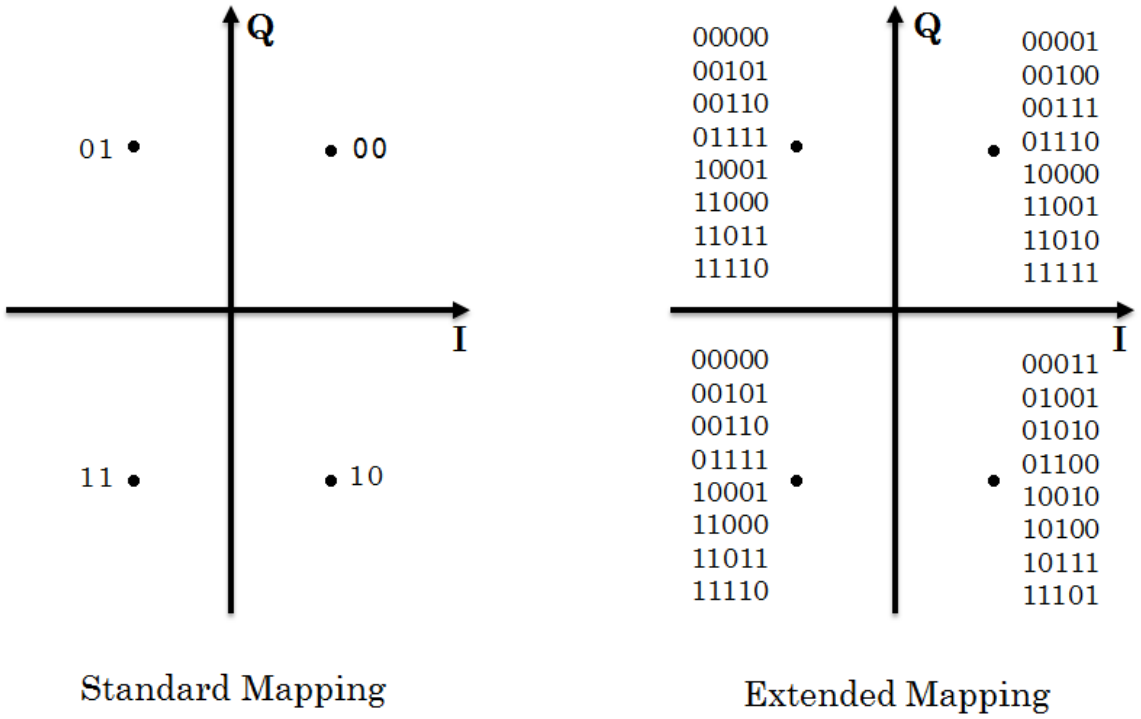

Figure 3.7: Difference between Standard and Extended Mapping

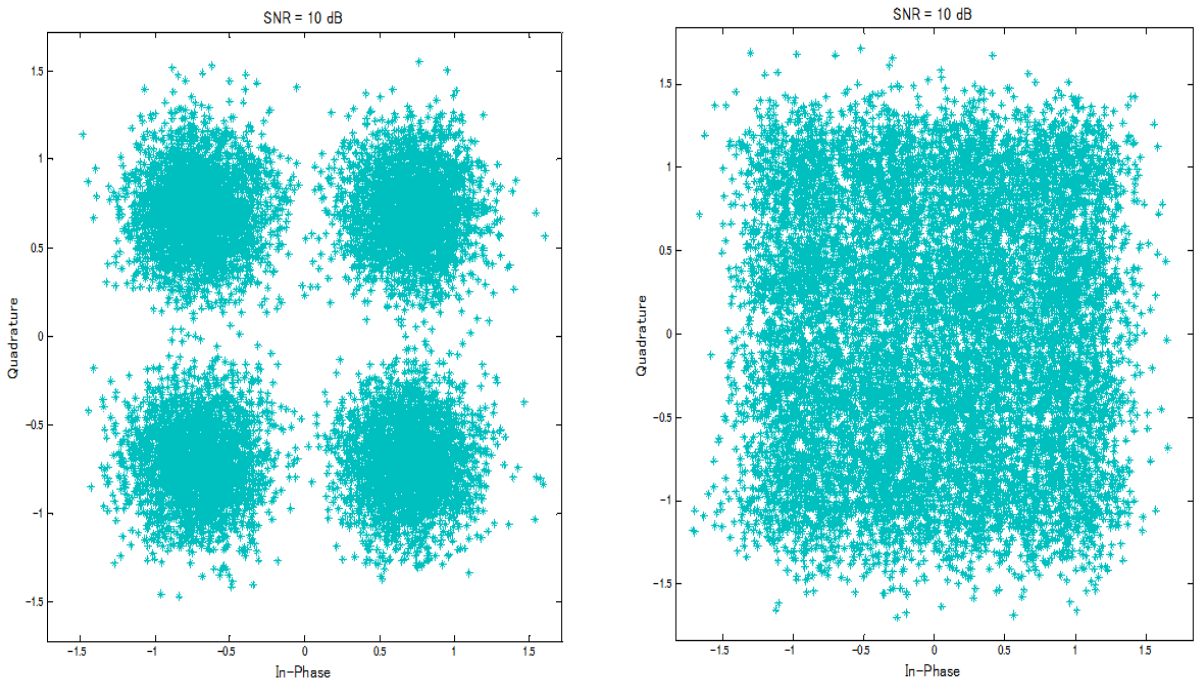

4-QAM 16-QAM

Figure 3.8: Noise Resistance Ability of SM and EM with $l_{map} = 4$

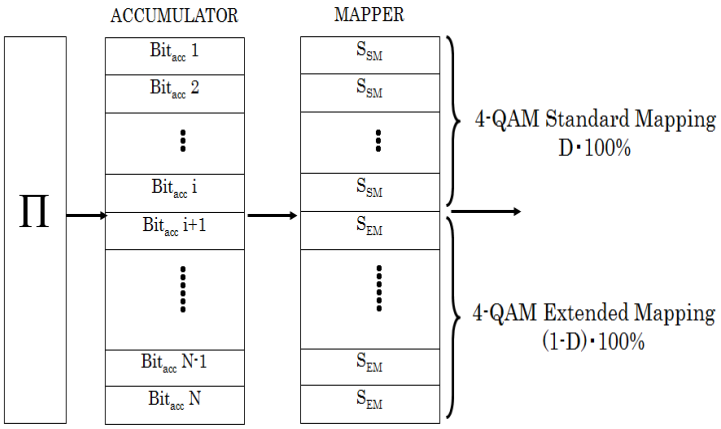

Figure 3.9: Modulation Doping on a Block of Code

combining. Fig. 3.9 illustrates a block diagram of the MD technique, where it is assumed that the interleaved bits sequence with length N is divided into K sub-blocks, and hence,

$$b_k^c = \alpha_k \cdot N \tag{3.16}$$

with

$$\sum_{k=1}^{K} \alpha_k = 1. \tag{3.17}$$

Each sub-block contains at least two coded bits. If D and $(1-D)$ are the ratios of the symbols with SM and EM, respectively, for a certain code block, the spectrum efficiency can be calculated as:

$$\eta_{SPCCIRC} = (D \cdot l_{SM} + (1-D) \cdot l_{map}) \cdot R_{SPCCIRC}. \tag{3.18}$$

3.2.4.4 Design of modulations

It has been shown by several researches that the signal mapping plays a very important role in determining the performance of BICM-ID system. Therefore, specific studies have been devoted for determining the mapping rule, e.g. Quadratic Assignment Problem (QAP)[5], Reactive Tabu Search (RTS) [6], Binary Switching Algorithm (BSA) [7]. They are the algorithms to determine the mapping rule from binary vectors to complex constellation points. Even the computational complexity of BSA grows rapidly when the order of modulation is increased, it has been widely used since BSA provides a solution to determine the labelling rules by simply considering the Euclidean distance between all possible pair of signals. It is well known that the labelling rules obtained by BSA is only the local optimal solution [7], since the labelling problems is highly non-linear. However,

Table 3.3: Binary Switching Algorithm

Algorithm 2 Binary Switching Algorithm (BSA)

repeat
  Generate labeling pattern L randomly empirically.
  Calculate the cost based on L
  Select the symbol s_{max} with maximum cost value Z.
  Pick the symbol s_{min} with second highest cost value by switching index between s_{max} and s_{min}
  if s_{min} exits. **then**
    Switch s_{max} and s_{min}
    Update Z regarding new L
  else
    Set s_{min} as s_{max}
  end if
until no existence of pair symbols for swapping

the local optimal solution obtained by BSA is very close to global optimal solution. The original BSA is described in Table. 3.3. It should be noted that to obtain near optimal labelling as the mapping rule, conducting original BSA for 100 loops has to be considered [17].

3.2.4.5 Joint Design of coding and modulation

The design of labelling pattern is performed, in general, with the aim of lifting up the right most part of the demapper curve to as high point of MI as possible. To achieve this goal, BSA is proposed by [7], as described above. However, since BSA does not take into account the matching between the demapper and decoder EXIT curves, there is still a possibility that the two curves intersect each other at a low point of MI. To solve this problem, Kisho Fukawa introduced, in his master thesis, a new technique, called EXIT-constraint Binary Switching Algorithm (EBSA), to achieve the desired optimal labelling mapping pattern. The EBSA, actually, can be seen as the combination of LP and BSA. This thesis re-outlines the algorithm in the following.

The summary of EBSA framework is shown in Table. 3.4. For the number of bit-per-symbol l_{map} and the number l_{ap} of known *a priori* information bit given, where

$$l_{ap} \in \{0, 1, \cdots, l_{map} - 1\}, \tag{3.19}$$

the labelling cost function Z_{ap} can be expressed as:

$$Z_{ap} = \frac{1}{l_{map} 2^{2(l_{map}-1)} 2^{l_{ap}}} \sum_{b=1}^{l_{map}} \sum_{s|s_b=0} \sum_{\hat{s}|\hat{s}_b=0} e^{-\frac{|\mu(s)-\mu(\hat{s})|^2}{\sigma_n^2}}, \tag{3.20}$$

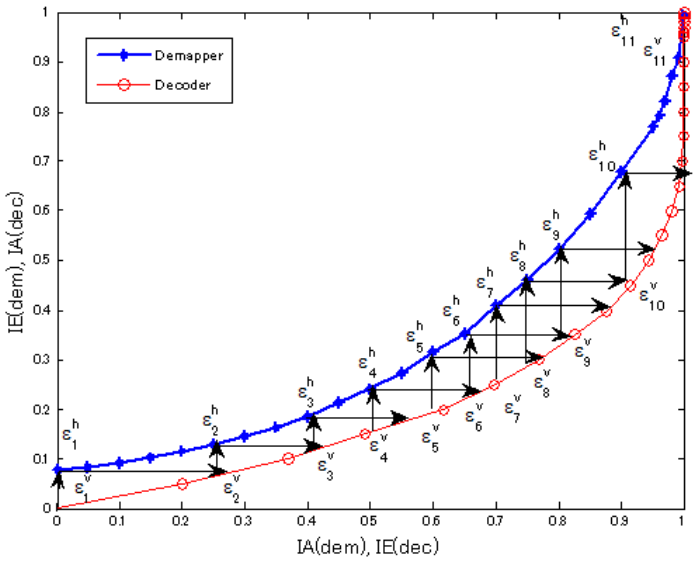

Figure 3.10: EBSA based Gaps Setting

where b is all the possible detected bits. s and $\hat{s}$ are the transmitted and received symbols differing only in the detected bit. The function $\mu(\cdot)$ returns the constellation points of those symbols. The total cost Z_t can be calculated by:

$$Z_t = \mathbf{Z} \cdot \lambda, \tag{3.21}$$

where the vector $\mathbf{Z} = [Z_0 \cdots Z_{l_{map}-1}]$ denotes the cost corresponding to the cases from no *a priori* information being known to the perfect *a priori* information being known. $\lambda = [\lambda_0 \cdots \lambda_{l_{map}-1}]^t$ defines the weight coefficient vector.

The EBSA, given in Table. 3.4 can jointly optimize the labelling rules, doping ratio for accumulator, and irregular degree allocations for the proposed BICM-ID system. Since EBSA considers both horizontal and vertical gaps between the demapper and decoder EXIT curves, a close matching between two curves, guaranteeing the convergence tunnel keeps open until (1.0, 1.0) of MI, is achievable. The example of horizontal and vertical gap setting are given in Fig. 3.10. Note that the horizontal gap, satisfying the horizontal gap constraint (ϵ_d^h), is obtained as a result of LP-based technique, while vertical gap, satisfying the vertical gap constraint (ϵ^ν), is obtained properly as a result of BSA; the bigger the cost value, the more the demapper EXIT curve will be pushed downwards, and vice versa. The effect of total labelling cost on demapper EXIT curve, $l_{map} = 5$ is shown in Fig. 3.11.

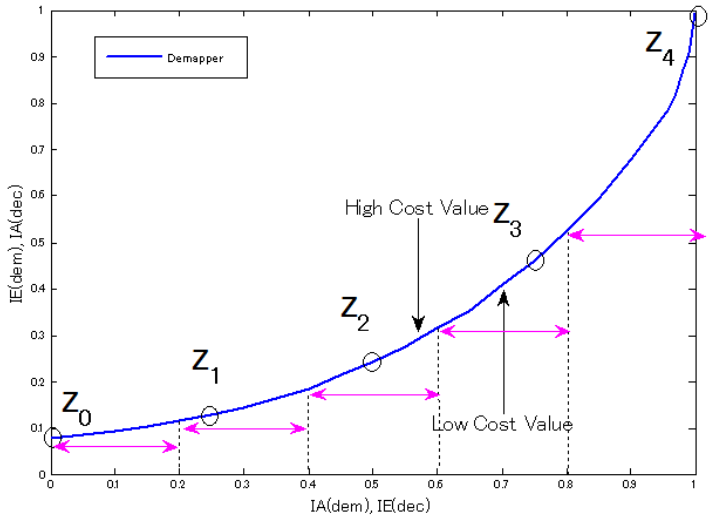

Figure 3.11: Effect of Labelling Cost on Demapper EXIT Curve

Table 3.4: EBSA Algorithm

Algorithm 3 EXIT-constrained Binary Switching Algorithm (EBSA)

Initialize the weight coefficient vector $\lambda_{ap} = [\lambda_0 \cdots \lambda_{l_{map}-1}] = [0 \cdots 1]$.
Initialize the desirable vertical epsilon values. e.g., $\epsilon^{\nu} = [0.001][1, \cdots, N_{desired\ point}]$.
Generate labeling pattern $\boldsymbol{L}$ randomly and degree distribution d_v empirically.
For $d_{acc} = 2$ and $d_c = 2$ **to** $d_{acc} = 100$ and $d_c = 100$, respectively **do**
Repeat
Draw demapper's EXIT curve based on labeling pattern $\boldsymbol{L}$.
for i = 1 **to** 100 **do**
Perform BSA using labeling pattern $\boldsymbol{L}$.
end for
Select the labeling pattern $\boldsymbol{M}$ with minimum cost from BSA.
Draw demapper EXIT curve and perform LP to determine the optimal node degree allocations.
Draw *LP-based* decoder EXIT curve and evaluate the horizontal gap (ϵ^h) between this two curves.
if the gap around Z_{ap} is larger than ϵ^{ν} **then**
$\lambda_{ap} = \lambda_{ap} - 1, \ \ 0 \leq \text{ap} \leq l_{map} - 1$
end if
Select the labeling pattern $\boldsymbol{M}$ and decoder's node degree distribution having the minimum gap.
Update labeling pattern $\boldsymbol{L}$ as $\boldsymbol{M}$.
Until the minimum gap is obtained
End for
Select the optimal parameters that minimize the gap

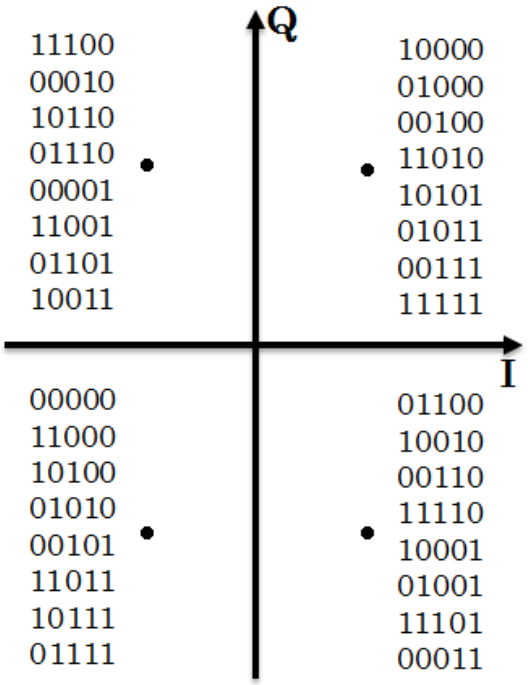

Figure 3.12: Balanced 4-QAM Extended Mapping Optimized at SNR = 0.8

Using the defined cost values and EBSA algorithm given in Table. 3.4, the optimal balanced labelling mapping rule for both 4-QAM and 16-QAM can be obtained. Fig. 3.12 and Fig. 3.13 illustrate the 4-QAM balanced labelling rules, with $l_{map} = 5$, which are optimized for SNR = 0.8 dB and SNR = 3.1 dB, respectively. Fig. 3.14, Fig. 3.15, and Fig. 3.16 are the labelling rule for 16-QAM, with $l_{map} = 6$, optimized at SNR = 2.0, 5.0, and 8.0 dB, respectively. The EXIT analysis and BER performance for the proposed system based on these labelling rules are given in **Chapter 5**.

3.2.5 Channel Model

Since the conditions of channel make a significant influence to the demapper for the demapping process, it is necessary to first understand the influence of the properties of the communication channels. The transmission impairments in wireless systems, caused by different practical issues, can be divided into three categories: They are related to (1) radio propagation from transmitter to receiver, (2) signal reception at the receiving antenna, and (3) the practical limitation of equipments used in real transceiver. There are typically two main types of channel used for investigating and designing systems; static and time-varying channels. The system performance in AWGN channel is dominated by SNR, while in fading channel, the transmitted signal suffers from terrain blocking, ground

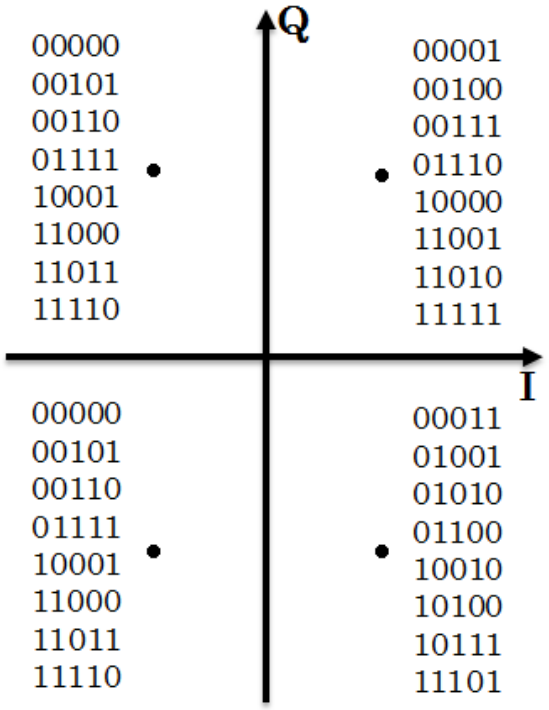

Figure 3.13: Balanced 4-QAM Extended Mapping Optimized at SNR = 3.1

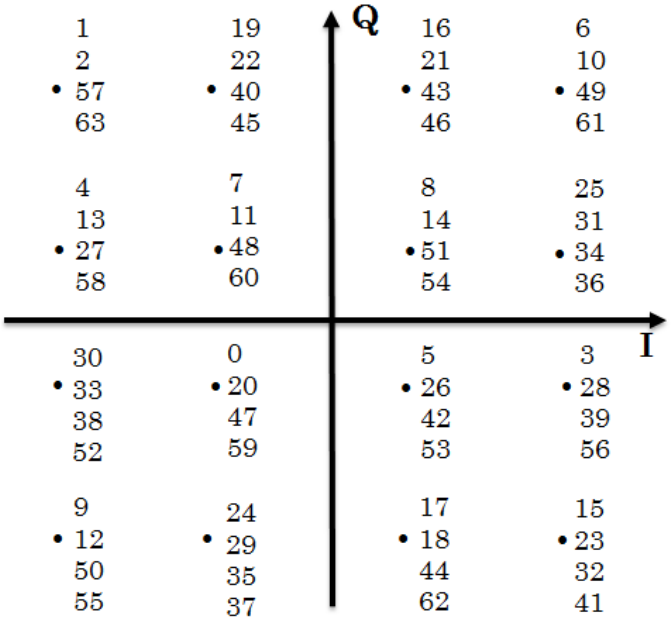

Figure 3.14: Balanced 16-QAM Extended Mapping Optimized at SNR = 2.0

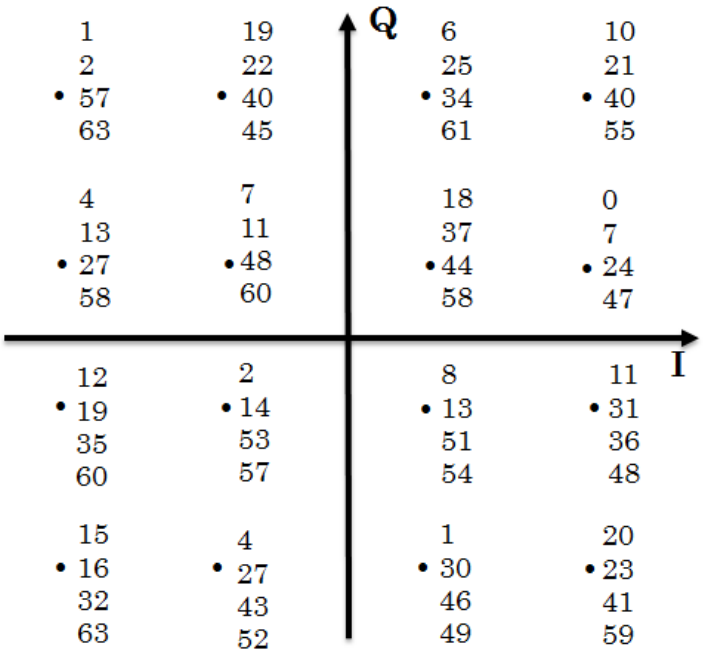

Figure 3.15: Balanced 16-QAM Extended Mapping Optimized at SNR = 5.0

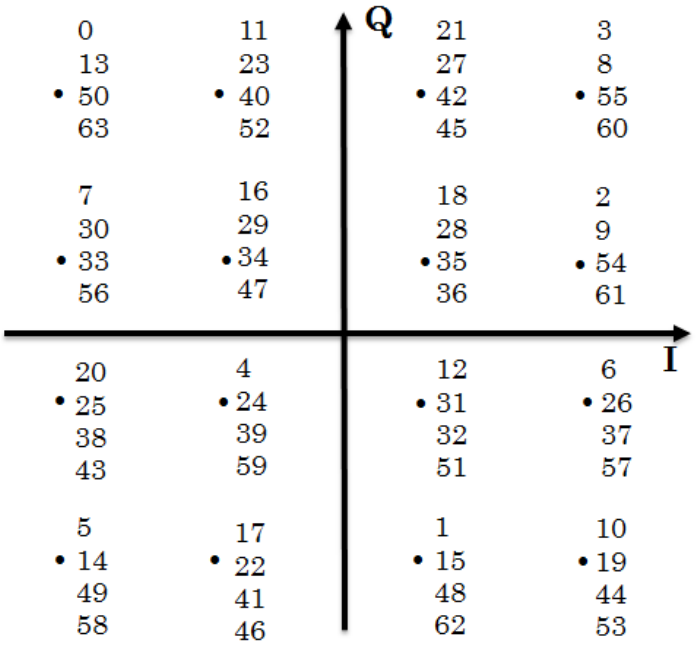

Figure 3.16: Balanced 16-QAM Extended Mapping Optimized at SNR = 8.0

clutter, multi-path, etc. The received signal r via the channel can be expressed as:

$$r(t) = h(t) \cdot x(t) + n(t), \tag{3.22}$$

where $h(t)$ and $x(t)$ are the complex channel and transmitted symbol at timing index t, respectively. $n(t)$ is a zero mean i.i.d AWGN with variance σ_n^2. In this thesis, block fading AWGN channel is always assumed for the simplicity, with which the channel gain $h(t) = 1$, and the SNR value can be properly controlled by changing the noise variance. Furthermore, the channel gain is constant over a block, and thus, this thesis omits the timing index t from $h(t)$. Note that the proposed technique can be extended to frequency selective fading channel by combining it with the turbo equalization techniques in order to remove the inter-symbol interference (ISI).

3.2.6 Demapper

As described above, since the proposed system assumes signal transmission over the AWGN channel, $h(t) \equiv 1$, and therefore, the received signal $r(t)$ at the receiver side is expressed as:

$$r(t) = x(t) + n(t), \tag{3.23}$$

where $x(t)$ and $n(t)$ are the transmitted modulated symbol and zero mean AWGN noise with variance σ_n^2, respectively, at a timing index t. For further simplicity, This thesis excludes the index t for the rest of the explanations. Note that, in order to have the received

signal with SNR, equivalent to $1/\sigma_n^2$, the transmitted signal is normalized, appropriately, according to the order of modulation format and/or signal constellation diagram.

Iterative demapping and decoding takes place at the receiver, where the *extrinsic* information is exchanged between the demapper and decoder, according to the Turbo principle. The *extrinsic* LLR, described in detail later, of the demapper output can be calculated by using the following equation:

$$L_{e,dem}[u_p] = \ln \frac{\sum_{s \in S_0} e^{(-\frac{|r-s|^2}{\sigma_n^2})} \prod_{q=1,q\neq p}^{l_{map}} e^{-u_q(s)L_a(u_q(s))}}{\sum_{s \in S_1} e^{(-\frac{|r-s|^2}{\sigma_n^2})} \prod_{q=1,q\neq p}^{l_{map}} e^{-u_q(s)L_a(u_q(s))}}, \tag{3.24}$$

where $S_0(S_1)$ and $L_a(u_q(s))$ denote the labelling set with p^{th} bit being 0(1) and the *a priori* LLR fed back from the decoder, respectively. q indicates the position of the bits allocated in the symbol s, while l_{map} corresponds to the number of bits in a symbol. It should be noted that the demapper output described above is derived based on maximum *aposteriori* probability (MAP) algorithm.

3.2.6.1 Turbo Principle

The Turbo code was firstly discovered by Berrou's group in 1993 [2]. It is known as a practical code that can achieved near capacity performance. The concept of the Turbo code is that, at the receiver side, the inner and outer codes are assumed to exchange *a priori* information with each other, via several iterations, in order to enhance the performance. What makes the approach of information exchange reasonably possible is the random interleaver which randomly spreads the coded bits from the original orders, yielding statistical independence between the output LLRs of inner and outer codes.

According to the information exchange, the LLR, described in next sub-section, is adopted. Given that there is no *apirori* information from outer code at the first iteration, the decoder of inner code initiates the decoding based on the received signal and channel knowledge only, and then provides the *extrinsic* output information to the outer decoder via interleaver as *a priori* information. The outer decoder then decodes the bit sequence using the *a priori* information from inner decoder, and feeds the *extrinsic* information via deinterleaver back to the inner decoder as *a priori* information. This process is performed iteratively until there is no more gain can be obtained through the exchange. After convergence, the outer decoder makes the hard decision based on *aposteriori* information. More detailed description of LLR is provided in the following sub-section.

3.2.6.2 Log Likelihood Ratio (LLR)

The LLR is used to provide a simple understanding of the information exchange between inner and outer decoders iteratively, following the turbo principle. The LLR of a data bit u_p can be defined as:

$$L(u_p) = ln\left(\frac{P(u_p = +1)}{P(u_p = -1)}\right) \tag{3.25}$$

with

$$P(u_p = +1) = \frac{e^{L(u_p)}}{1 + e^{L(u_p)}} \quad (3.26)$$

$$= \frac{1}{1 + e^{-L(u_p)}} \quad (3.27)$$

and

$$P(u_p = -1) = \frac{1}{1 + e^{L(u_p)}} \quad (3.28)$$

$$= \frac{e^{-L(u_p)}}{1 + e^{-L(u_p)}}. \quad (3.29)$$

$P(u_p = +1)$ and $P(u_p = -1)$ indicate the probabilities of the coded bit u_p being 0 and 1, respectively. Note that when the LLR $L(u_p) \approx 0$, the probabilities of $P(u_p = +1) \approx P(u_p = -1) \approx 0.5$, and therefore, uncertainty about u_p is very high in this case. In other words, the enough knowledge about u_p is achieved if $P(u_p = +1) \gg P(u_p = -1)$, yielding $L(u_p) \gg 0$. In the same way, $L(u_p) \ll 0$ if $P(u_p = +1) \ll P(u_p = -1)$. Fig. 3.17 shows the relationship between The LLR $L(u_p)$ and the probability $P(u_p = +1)$.

There are three types of LLR based information used in the information exchange between the inner and outer decoders.

- *a priori* information (L_a): it indicates the amount of already known information, provided by the other decoders or the decoders of other users in the multiple access channel transmission scheme before decoding.
- *extrinsic* information (L_e): it is the information, output from demapper or inner decoder, obtained by using the channel values and *a priori* information by the other outer decoder. The *extrinsic* information output from the outer decoder can be calculated by subtracting *a priori* information from the *a posteriori* information, output from the outer decoder.
- *aposteriori* information (L_p): it represents the total amount of information, L_a plus L_e at the decoder output.

3.2.7 BCJR Decoder

The Bahl-Cocke-Jelinek-Raviv (BCJR) decoding algorithm was originally introduced in [9] in the late 1974. It is used, in general, for performing MAP decoding of trellis based error correction codes, e.g. convolutional codes or trellis coded modulation. Decoding process for the partial accumulator used in the proposed system requires the BCJR algorithm, because it is a very simple recursive rate-1 convolutional code.

LLR based on the MAP of a data bit u_p, under the conditions of channel, is defined as:

$$L(u_p|\boldsymbol{r}) = ln\left(\frac{P(u_p = +1|\boldsymbol{r})}{P(u_p = -1|\boldsymbol{r}}\right), \quad (3.30)$$

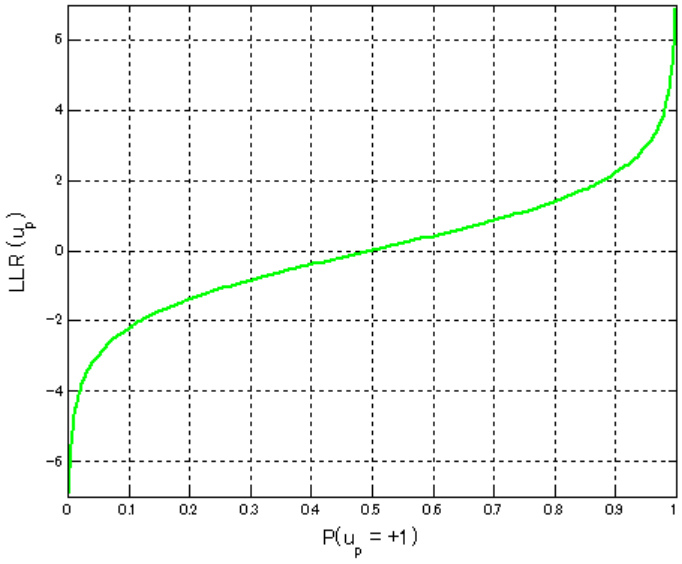

Figure 3.17: Relationship between $LLR(u_p)$ and $P(u_p = +1)$

where $\boldsymbol{r} = (r(1), \cdots, r(N))^t$ denotes the received signal vector. $P(u_p = +1|\boldsymbol{r})$ and $P(u_p = -1|\boldsymbol{r})$ are the appearance probabilities of two possible bit values, 0 and 1, for the bit u_p given that $\boldsymbol{r}$ is known. The 2-state trellis diagram is shown Fig. 3.18 as an example. Given that s_p and s_{p-1}, the present state and the previous state in the trellis diagram, respectively, are known, then, the equation (3.30) can be redefined as [12]:

$$L(u_p|\boldsymbol{r}) = ln\left(\frac{P(u_p = +1|\boldsymbol{r})}{P(u_p = -1|\boldsymbol{r}}\right) \tag{3.31}$$

$$= ln\left(\frac{\sum_{(s_{p-1},s_p)\to U_p^+} P(s_{p-1}, s_p, \boldsymbol{r})}{\sum_{(s_{p-1},s_p)\to U_p^-} P(s_{p-1}, s_p, \boldsymbol{r})}\right), \tag{3.32}$$

with

$$P(s_{p-1}, s_p, \boldsymbol{r}) = P(s_{p-1}, s_p, \boldsymbol{r}_{t<p-1}, r_{p-1}, \boldsymbol{r}_{t>p-1}) \tag{3.33}$$

$$= P(s_{p-1}, \boldsymbol{r}_{t<p-1}) \cdot P(s_p, r_{p-1}|s_{p-1}) \cdot P(\boldsymbol{r}_{t>p-1}|s_p) \tag{3.34}$$

$$= \alpha_{p-1}(s_{p-1}) \cdot \gamma_{p-1}(s_{p-1}, s_p) \cdot \beta_p(s_p), \tag{3.35}$$

where $(s_{p-1}, s_p) \to U_p^+$ represents the all transitions of state pairs for the bit $u_p = +1$ at timing index p. $\boldsymbol{r}_{t<p-1}$ and $\boldsymbol{r}_{t>p-1}$ collect the samples of the received signal $\boldsymbol{r}$ before and after timing index $(p-1)$, respectively. The probability of *forward recursion* for each state s at timing index $p-1$, $\alpha_{p-1}(s_{p-1})$, can be redefined as:

$$\alpha_p(s_p) = P(s_p, \boldsymbol{r}_{t<p}) \tag{3.36}$$

$$= \sum_{s_{p-1}} \gamma_{p-1}(s_{p-1}, s_p) \cdot \alpha_{p-1}(s_{p-1}), \tag{3.37}$$

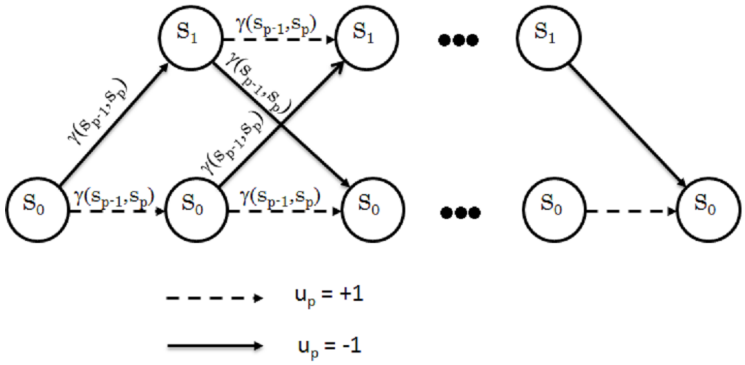

Figure 3.18: 2-State Trellis Diagram

with the initialization of starting state at time $p = 1$, by

$$\alpha_0(s_p) = \begin{cases} 1, s_p = 0 \\ 0, s_p \neq 0. \end{cases} \tag{3.38}$$

Similarly, the *backward recursion* $\beta_p(s_p)$ can be calculated by:

$$\begin{aligned} \beta_{p-1} &= P(\boldsymbol{r}_{t>p-2}|s_{p-1}) && (3.39) \\ &= \sum_{s_p} \gamma_{p-1}(s_{p-1}, s_p) \cdot \beta_p(s_p) && (3.40) \end{aligned}$$

with the initial condition at the timing index $p = T + 1$, by

$$\beta_{T+1}(s_p) = \begin{cases} 1, s_p = 0 \\ 0, s_p \neq 0. \end{cases} \tag{3.41}$$

For the *branch matrix* $\gamma_{p-1}(s_{p-1}, s_p)$, it is rewritten as:

$$\begin{aligned} \gamma_{p-1}(s_{p-1}, s_p) &= P(u_{p-1}) \cdot P(r_{p-1}|b_{p-1}) && (3.42) \\ &= e^{\frac{L_j^u + L_j^c}{2}} && (3.43) \end{aligned}$$

with

$$L_j^u = \begin{cases} L_{e,dem,j} + L_{e,dec,j}, & j \ mod \ P \neq 0 \\ L_{e,dec,j}, & j \ mod \ P = 0 \end{cases} \tag{3.44}$$

and

$$L_j^c = \begin{cases} 0, & j \ mod \ P \neq 0 \\ L_{e,dem,j}, & j \ mod \ P = 0, \end{cases} \tag{3.45}$$

where L_j^u and L_j^c denote the LLR values of uncoded and coded bits at the timing index j, respectively. P is the doping ratio of the partial accumulator. Fig. 3.19 and Fig. 3.20

Table 3.5: BCJR Algorithm

Algorithm 4 BCJR Algorithm
Initialize $\tilde{\alpha_0}$ and $\tilde{\beta}_{T+1}$
Calculate the log-based branch matrices $\tilde{\gamma}_{p-1}(s_{p-1}, s_p)$ based on (3.43)
Estimate the log-based $\tilde{\alpha}_{p-1}(s_{p-1})$ using (3.37)
Fine the value of (3.40) based *backward* matrices $\tilde{\beta}_p(s_p)$
Compute the *a posteriori* information using (3.49)

depict the *forward recursion* and *backward recursion* for the trellis diagram shown in Fig. 3.18. In order to solve the problem due to the numerical instability, including overflow and underflow that may occurs when calculating equation (3.32), it is preferred to transform the MAP algorithm to the logarithmic domain. Using the following relationship:

$$\tilde{\alpha}_{p-1}(s_{p-1}) = ln(\alpha_{p-1}(s_{p-1})), \tag{3.46}$$

$$\tilde{\gamma}_{p-1}(s_{p-1}, s_p) = ln(\gamma_{p-1}(s_{p-1}, s_p)), \tag{3.47}$$

$$\tilde{\beta}_p(s_p) = ln(\beta_p(s_p)), \tag{3.48}$$

the equation (3.32) can be rewritten by:

$$L(u_p|r) = ln\left(\frac{\sum_{(s_{p-1},s_p)\to U_p^+} e^{\tilde{\alpha}_{p-1}(s_{p-1})+\tilde{\gamma}_{p-1}(s_{p-1},s_p)+\tilde{\beta}_p(s_p)}}{\sum_{(s_{p-1},s_p)\to U_p^-} e^{\tilde{\alpha}_{p-1}(s_{p-1})+\tilde{\gamma}_{p-1}(s_{p-1},s_p)+\tilde{\beta}_p(s_p)}}\right), \tag{3.49}$$

where the calculation of $ln(\sum_T e^{\Psi_T})$ can rely on Jacobian algorithm in [14]:

$$ln(e^{\Psi_1} + e^{\Psi_2}) = max(\Psi_1, \Psi_2) + ln(1 + e^{-|\Psi_1 - \Psi_2|}). \tag{3.50}$$

The algorithm using Equation (3.46) - (3.50) is called Max-log-MAP with compensation factor (or log-MAP). Note that the second term on the right hand side of equation (3.50) is eliminated in the Max-log-MAP algorithm. This is preferable if the appearance probabilities of the *a priori* information bits are equally likely, since the computational complexity of this algorithm is lower than that of the log-MAP algorithm. However, this thesis always employs the log-MAP algorithm for the simulations, since the large variation of *a priori* information of coded bits are assumed, and in order to approach the capacity as close as possible. It is desirable that all determined fators, including approximations, should be avoided, so far as the complexity stays at a practical level. The log-domain BCJR algorithm is summarized in Table. 3.5.

3.2.8 Channel Coding Decoder

Since the SPCC and IRC are used, their decoding processes are different part by part, according to the variable node and check node degrees. The decoder structure is depicted

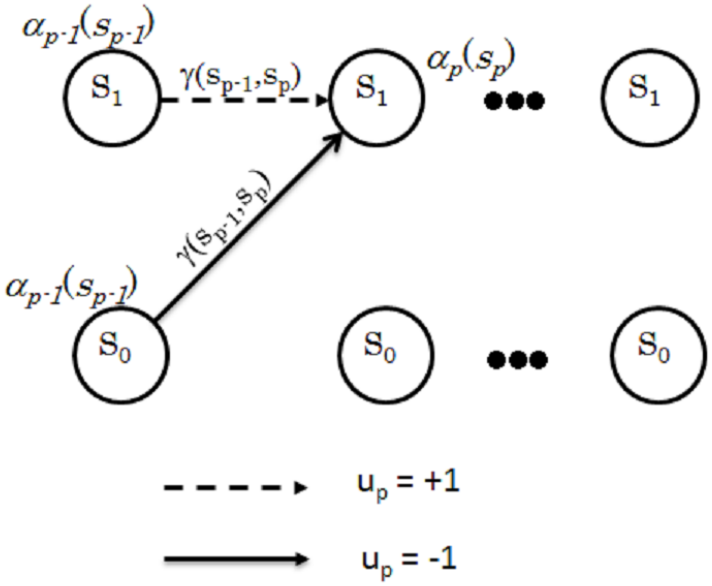

Figure 3.19: Forward Recursion

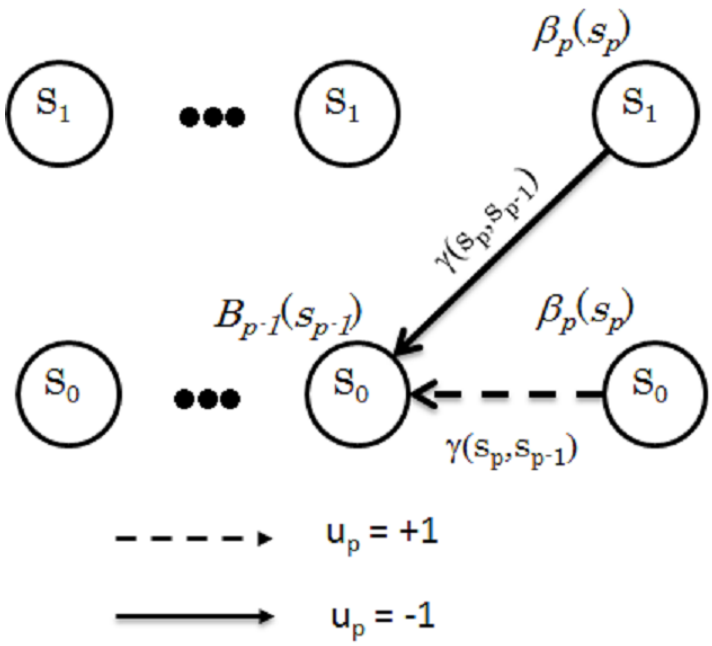

Figure 3.20: Backward Recursion

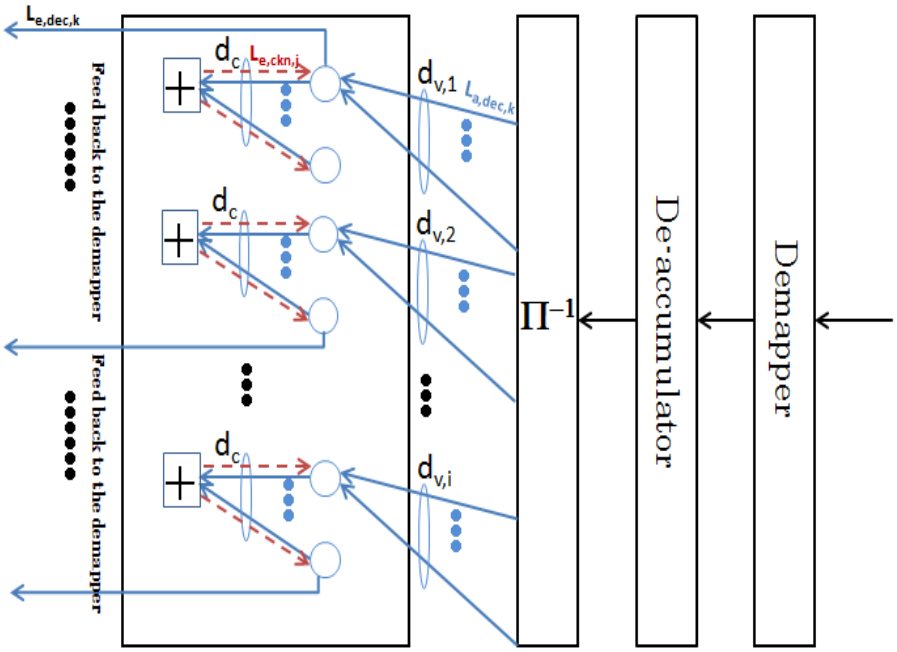

Figure 3.21: Structure of SPCCIRC Decoder

in Fig. 3.21, where the *extrinsic* LLR of the decoder output, to be fed back to the demapper via interleaver, can be calculated by:

$$L_{e,dec,k} = L_{e,ckn,j} + \sum_{i=1,i\neq k}^{d_{(v,i)}} L_{a,i} \tag{3.51}$$

with

$$L_{e,ckn,j} = \sum_{w=1,w\neq j}^{d_c} \boxplus L_{a,ckn,w}, \tag{3.52}$$

where, because of the irregular structure of the repetition code, the variable node degree $d_{(v,i)}$ has several values which is indexed by i. d_c represents the check node degree. $L_{a,i}$ indicates the *a priori* LLR, which is equivalent to the deinterleaved *extrinsic* LLR, output from the demapper. The check node box-sum operator in equation (3.52) can be referred to [8]. The rate of the code R is calculated by equation (3.5).

Note that the calculation of MI of *extrinsic* LLR output can rely on equation (2.23). Assuming Gaussian distribution for the LLR, the MI of *extrinsic* output of the SPCC-IRC decoder $I_{e,dec,j}$ can be expressed by using J-function as:

$$I_{e,dec,j} = \frac{\sum_i \alpha_i \cdot d_{v,i} \cdot J(\sqrt{(d_{v,i}-1)\cdot J^{-1}(I_{a,dec,k})^2 + J^{-1}(I_{e,ckn,j})^2})}{\sum_i \alpha_i \cdot d_{v,i}} \tag{3.53}$$

Table 3.6: The Computational Complexity of Demapper and Decoder per Symbol Output ($(\tau = l_{map})$ is used because of the space limitation)

	Addition/Subtraction	Multiplication	Division
Demapper	$\tau \cdot (2^{\tau-1} + \tau - 1)$	$\tau^2 \cdot 2^{\tau-1} - \tau$	$2^{\tau-2}$
Decoder	$2 \cdot d_v \cdot \tau$	$(d_c - 2) \cdot \tau$	0

with

$$I_{e,ckn,j} = 1 - J(\sqrt{d_c - 1} \cdot J^{-1}(1 - I_{a,ckn,j})), \tag{3.54}$$

where

$$I_{a,ckn,j} = J(\sqrt{d_{v,i} \cdot J^{-1}(I_{a,dec,k})^2}). \tag{3.55}$$

$I_{a,ckn,j}$ and $I_{e,ckn,j}$ represent the MI of the *a priori* and *extrinsic* LLR of the check node decoder, respectively. $I_{a,dec,k}$ denotes the MI of the *extrinsic* LLR of demmapper, to be provided to the decoder via the deinterleaver.

3.2.9 Computational Complexity of the System

The complexity of the proposed system are mainly due to the demmaper and the decoder. The computational complexity of both demapper and decoder are summarized in Table. 3.6. The complexity of 4-QAM with $l_{map} = 5$, and 16-QAM with $l_{map} = 6$ for the demapper are discussed in the following:

- **4-QAM**: Given $l_{map} = 5$, there are $2^5 = 32$ labelling patterns, in total, in the signal constellation diagram. Since the demapper calculation is performed in the log domain which divides the labelling patterns into numerator and denominator of equation (3.24), each having 16 labelling patterns, this is equivalent to the complexity of the BCJR algorithm with two processes, forward and backward recursion. Therefore, with $l_{map} = 5$, the computational complexity is equivalent to the BCJR algorithm based decoding of convolutional code using memory-3 ($\log_2(\frac{16}{2}) = \log_2(8) = 3$). However, since two constituent convolutional codes is needed in the Turbo code [2], the complexity of demapper becomes roughly the same level of that for the Turbo code having two constituent codes with memory-2.

- **16-QAM**: Similarly to the case of 4-QAM, with $l_{map} = 6$, there are $2^6 = 64$ labelling patterns in constellation diagram, in total, for 16-QAM. Then, the complexity of 16-QAM can be calculated as $\log_2(\frac{32}{2}) = \log_2(16) = 4$, and therefore, it is equivalent to the complexity of the BCJR algorithm based decoding of convolutional code using memory-4 which is only equivalent to the Turbo code with two constituent convolutional codes with memory-3.

Note that the computational complexity of the original Turbo code proposed by C. Berrou in [2] is roughly 4 times and 2 times as large as the proposed system with 4-QAM and 16-QAM, respectively, since [2] uses two constituent convolutional codes with memory-4. If the computational complexity with the BCJR-decoding based deaccumulator, equivalent to convolutional code with memory-1, is taken into account, the complexity of [2] still remains roughly 4 times and 2 times, respectively, as high as the proposed system with 4-QAM and 16-QAM, because the complexity due to the deaccumulator is almost negligible compared to the demapper part. However, the BER performances, shown later in **Chapter 4**, of the proposed system are better than [2]. Therefore, it can be concluded that the proposed system beats [2] in terms of performance and complexity.

Chapter 4

Interleave Division Multiple Access (IDMA)

In this chapter, the research on BICM-ID based Interleave Division Multiple Access (IDMA) is presented. It provides, first of all, the fundamental knowledge about IDMA which covers basic technique, advantage/disadvantage, as well as comparison between IDMA and Code Division Multiple Access (CDMA). After that, the investigations over the single user detection and multiple user detection techniques are described in two independent sections, respectively. It is shown that a channel coding can be designed by a single low rate code without any spreading sequence like CDMA technique requires, and therefore, the spectrum can be fully and directly allocated to the channel coding with the proposed IDMA.

4.1 IDMA Principle

IDMA is one of the powerful multiple access schemes which is considered one of the most promising candidates for the uplink in future wireless communication systems. It separates users at the chip level by random inteleavers, and uses low rate code as a channel coding with iterative multiple users detection and decoding at the receiver side. Fig. 4.1 illustrates the system model of the conventional IDMA. The information from each user is encoded by forward error control (FEC) encoder, interleaved by random interleaver yielding i.i.d binary sequence of users, and then transmitted through multiple access channel. The received signal $r(j)$, at the receiver side, can be expressed as:

$$r(j) = h_k(j) \cdot x_k(j) + \xi_k(j) \tag{4.1}$$

with

$$\xi_k(j) = \sum_{g \neq k, g=1}^{K} h_g(j) \cdot x_g(j) + n(j), \tag{4.2}$$

where $h_k(j)$ and $x_k(j)$ denote the channel fading coefficient and the transmitted symbol for user k at timing index j, respectively. $\xi_k(j)$ represents the interference from other

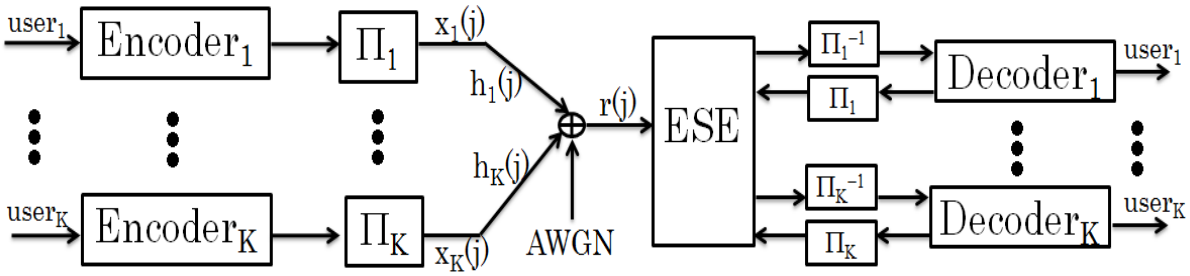

Figure 4.1: Conventional IDMA

users plus noise, and $n(j)$ is the zero mean AWGN channel with variance σ_n^2. Note that according to the central limit theorem, $\xi_k(j)$ can be approximated by Gaussian-distributed noise having mean $E(\xi_k(j))$ and variance $Var(\xi_k(j))$ which is used to estimate the transmitted signal $x_k(j)$ at the receiver side. The information exchange between elementary signal estimator (ESE) and the decoders are performed iteratively following the turbo concept. It should be noted that in each iteration the mean and variance of $\xi_k(j)$ is updated based on the output of the decoder.

There are typically two ways to design the channel coding technique for IDMA. One is by combining a conventional convolutional code and a simple repetition code or spreading code. The other is to design a very low rate code to directly use the full bandwidth allocated for the transmission scheme. Both of them rely on the iterative detection and decoding technique following the turbo principle [2]. This thesis concentrates on designing only a very low rate irregular repetition code, based on the techniques described in the previous chapter, without mixing any other codes.

4.2 IDMA vs. CDMA

Since IDMA has a close relationship with CDMA, before going into the details about IDMA, it is worth to know what is CDMA, and how they correlate with each other. This section provides a simple understanding of CDMA in brief, as well as its pros and cons. In addition, the comparison between CDMA and IDMA , in general, will be described. This section also covers the reason why CDMA is widely used, and IDMA becomes a new better candidate for future wireless communication in stead of CDMA.

4.2.1 Introduction to CDMA

In general, if people wish to talk to each other simultaneously, they can choose whether to speak in turn, talk at the different pitches, or speak in different languages, to avoid the interruption from others. These choices correspond to time division multiple access (TDMA), frequency division multiple access (FDMA), and code division multiple access (CDMA), respectively. CDMA is widely used in the 3G communication systems which

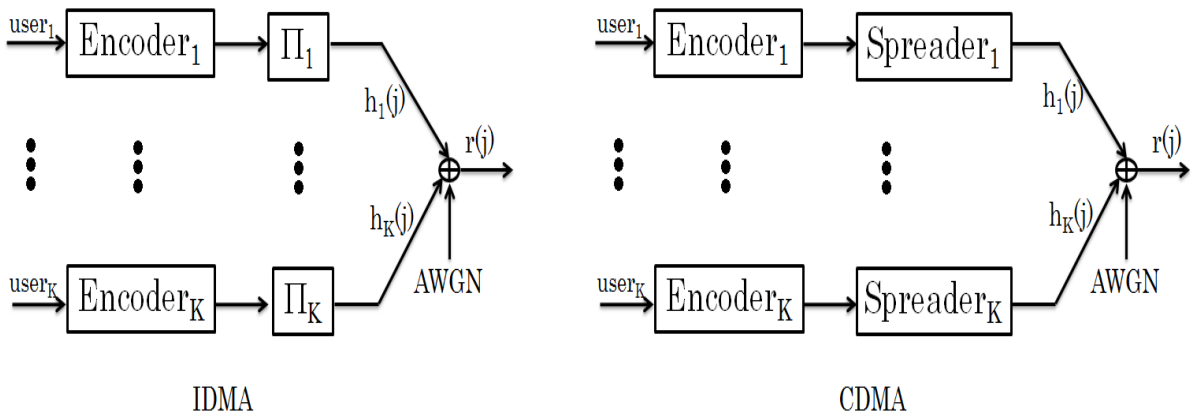

Figure 4.2: Conventional CDMA vs. IDMA at the Transmitter

is known as the direct sequence spread spectrum multiple access. It was originally introduced on the purpose of supporting simultaneously several data transmission, at a time, under the a certain condition of communication channels. This concept allows numerous users to share a bandwidth or a band of frequency without significant correlations among the users, due to the different assignment of spreading sequences to each transmitter. In the Fig. 4.2, the traditional system model of CDMA compared with IDMA, at the transmitter, is depicted. It can be seen that the only difference is that CDMA uses spreading sequence to distinguish the users, while IDMA directly employs the random interleaver to assure the independent among users. They look similar to each other, but the complexity of detection and decoding at the receiver, as well as the performance are completely different. Performance of IDMA, shown later, outperforms CDMA over frequency flat fading channels.

4.2.2 Comparison of IDMA and CDMA

IDMA actually can be seen as a transmission technique derived based on CDMA, which the concatenation of repetition code and interleaver works as the so-called spreading sequence in CDMA. IDMA distinguishes users by using only random interleaver, and therefore, a full bandwidth can be, directly, expanded for the channel coding only. IDMA also inherits several advantages from CDMA, e.g. the diversity against the frequency selective Rayleigh fading channel, diminishing of inter-user interference problems. However, since any statistical signal processing-based user separation and path energy combining, such as minimum mean square error (MMSE) detection technique is not used at the receiver side, the computational complexity of IDMA only grows linearly according to the increase in simultaneous users. The computational complexity with MMSE detector based CDMA grows $\mathbf{O}(K^2)$ [18], with K being the number of users. From the observations described above, IDMA is considered as one of the most promising multiple access techniques for next generation of cellular communication systems.

4.3 BICM-ID based IDMA

4.3.1 Design of Low Rate Code

Up until the previous section, a lot of advantageous points of the EBSA-aided SPCC-IRC BICM-ID technique have been presented. This sub-section, as well as the following sub-sections, exploit those advantageous point to design the IDMA system. In fact, this sub-section utilizes EBSA for designing the low rate code and labelling patterns for IDMA systems. However, since with the very low rate code, the demapper EXIT curve results in a very low starting point of MI due to the ambiguity of several labellings in a signal constellation with EM as well as the increase in number of users, the MD technique is also adopted in this thesis. In addition, due to the complexity for demapping grows according to the increase in number of simultaneous users, as a primary investigation, $l_{map} = 4$ is considered. Fig. 4.3 shows the balanced labelling rule, $l_{map} = 4$, obtained by EBSA. Note that this labelling pattern is designed on the purpose of pushing up the left most part of the demapper EXIT curve to as high point of MI as possible, in order to avoid an early intersection, at a low MI point, between the demapper and decoder EXIT curves in the multiple users detection scheme. Therefore, the initialization of the weight coefficient vector λ_{ap}, $\lambda_{ap} = [\lambda_0, \cdots, \lambda_{map-1}]$, is predefined as $\lambda_{ap} = [1\ 0\ \cdots\ 0\ 1]$. Note that even though the demapper EXIT curve can reflexively be changed by EBSA to obtain an optimal labelling pattern, there is a limit that EBSA can design a labelling rule that can lift up the demapper curve to the desirably high MI point, under a certain condition of SNR and l_{map}. Moreover, it is found that even using the designed labelling rule with a starting MI point higher than that presented in the previous chapter, the intersection point of the two curves remains at the low point of MI, according to the increase in number of users. Hence, the MD technique is also applied in this thesis. Since MD technique uses at least two labelling mapping patterns to map symbols on constellations, standard non-Gray mapping, illustrated in Fig. 4.4, is adopted as the combination between the labelling pattern described above in Fig. 4.3.

4.3.2 Single User Detection (SUD)

Fig. 4.5 illustrates the structure of the proposed BICM-ID based IDMA system with single user detection (SUD). The binary bit information sequence $b_{k,i}$ of user-k, $k \in \{1, \cdots, K\}$, at the timing index i is encoded by channel encoder using SPCC and IRC. The encoded bit sequence is bit-interleaved by a random interleaver Π_k, and then accumulated by partial accumulator to generate a new bits sequence $u_{k,j}$. The accumulated binary sequence $u_{k,j}$ are mapped using two different signal constellation diagrams, depicted in Fig. 4.3 and Fig. 4.4, to produce transmission symbols $x_{k,m}$. The symbols are transmitted over frequency-flat fading channels $h_{k,m}$. At the receiver, received signal r_m at the timing index m can be expressed as:

$$r_m = \sum_{k=1}^{K} \sqrt{P_k^w} \cdot h_{k,m} \cdot x_{k,m} + n_m, \tag{4.3}$$

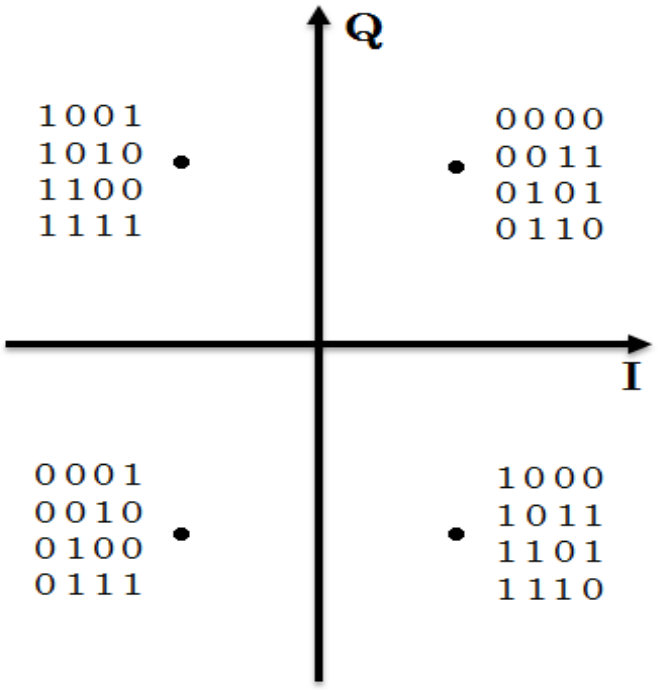

Figure 4.3: 4-QAM Extended Mapping with $l_{map} = 4$

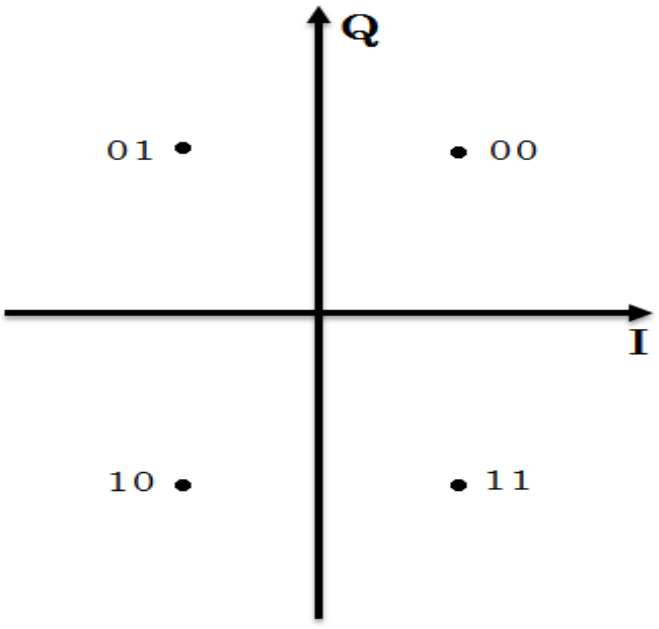

Figure 4.4: 4-QAM Standard Non-Gray Mapping with $l_{map} = 2$

where P_k^w and n_m denote the power allocated to the k^{th} user and the zero mean AWGN component with variance σ_n^2, respectively. By assuming that the interference from other users is equivalent to noise, when concentrating on user-k, equation (4.3) can be rewritten as:

$$r_m = \sqrt{P_k^w} \cdot h_{k,m} \cdot x_{k,m} + \zeta_{k,m} \tag{4.4}$$

with

$$\zeta_{k,m} = \sum_{g \neq k, g=1}^{K} \sqrt{P_g^w} \cdot h_{g,m} \cdot x_{g,m} + n_m, \tag{4.5}$$

where $\zeta_{k,m}$ indicates the multiple access interference (MAI) from the other users plus AWGN. If the number of users K is assumed to be large enough, $\zeta_{k,m}$ in equation (4.4) can be approximated as a Gaussian random variable according to the central limit theorem. Thus, the total noise variance of the k^{th} user, $\sigma_{k,\zeta,m}^2$, at the timing index m is expressed as:

$$\sigma_{k,\zeta,m}^2 = \sum_{g \neq k, g=1}^{K} P_g^w \sigma_{g,x,m}^2 + \sigma_n^2. \tag{4.6}$$

The *extrinsic* information exchange between demapper and decoder is performed iteratively, at the receiver side, adhering the turbo principle. The *extrinsic* LLR $L_{k,e,dem}$ of the demapper output of the d^{th} bit in labelling vector corresponding to the transmitted symbol can be expressed as:

$$L_{k,e,dem}[b_{k,d}] = \ln \frac{\sum_{s \in S_0} e^{(-\frac{|r_m - s|^2}{\sigma_{k,\zeta,m}^2})} \prod_{q=1, q \neq d}^{l_{map}} e^{-b_q(s) L_{k,a,dem}(b_q(s))}}{\sum_{s \in S_1} e^{(-\frac{|r_m - s|^2}{\sigma_{k,\zeta,m}^2})} \prod_{q=1, q \neq d}^{l_{map}} e^{-b_q(s) L_{k,a,dem}(b_q(s))}}, \tag{4.7}$$

where $S_0(S_1)$ and $L_{k,a,dem}(b_{k,q}(s))$ denote the labelling set, of which the d^{th} bit is 0(1) and the *a priori* LLR fed back from the decoder, respectively. $L_{k,a,dem}$ here, as can be seen from Fig. 4.5, is equivalent to *extrinsic* information of decoder $L_{k,e,dec}$ forwarded via the deinterleaver. q indicates the position of the bits allocated in the symbol s. Note that the demapper calculation above is evaluated based on the MAP criterion. The EXIT analysis and BER performance evaluation of IDMA with SUD technique is presented in **Chapter 5**

4.3.3 Multiple User Detection (MUD)

Fig. 4.6 shows a block diagram of the system of the proposed BICM-ID based IDMA with multiple user detection (MUD). It can be seen clearly here that, at the transmitter side, it is exactly the same as the case of SUD technique described above. Therefore, the received signal r_m, at the receiver side, is also the same as the case of SUD, as:

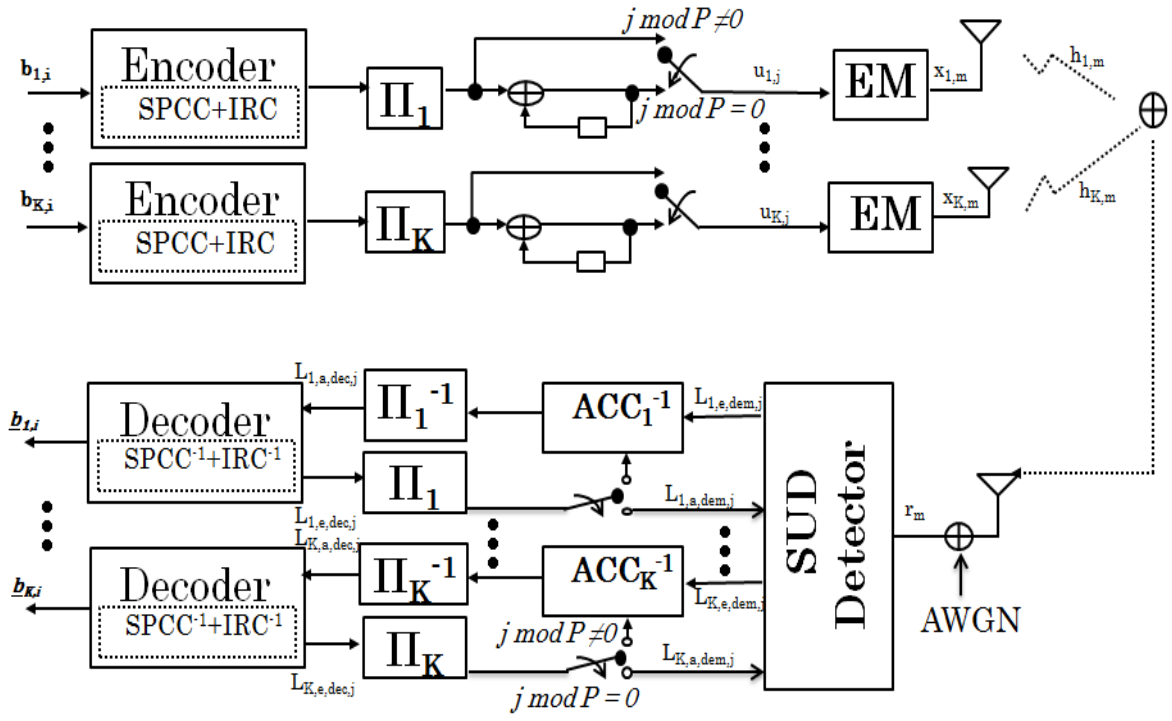

Figure 4.5: System Model of Proposed IDMA with Single User Detection

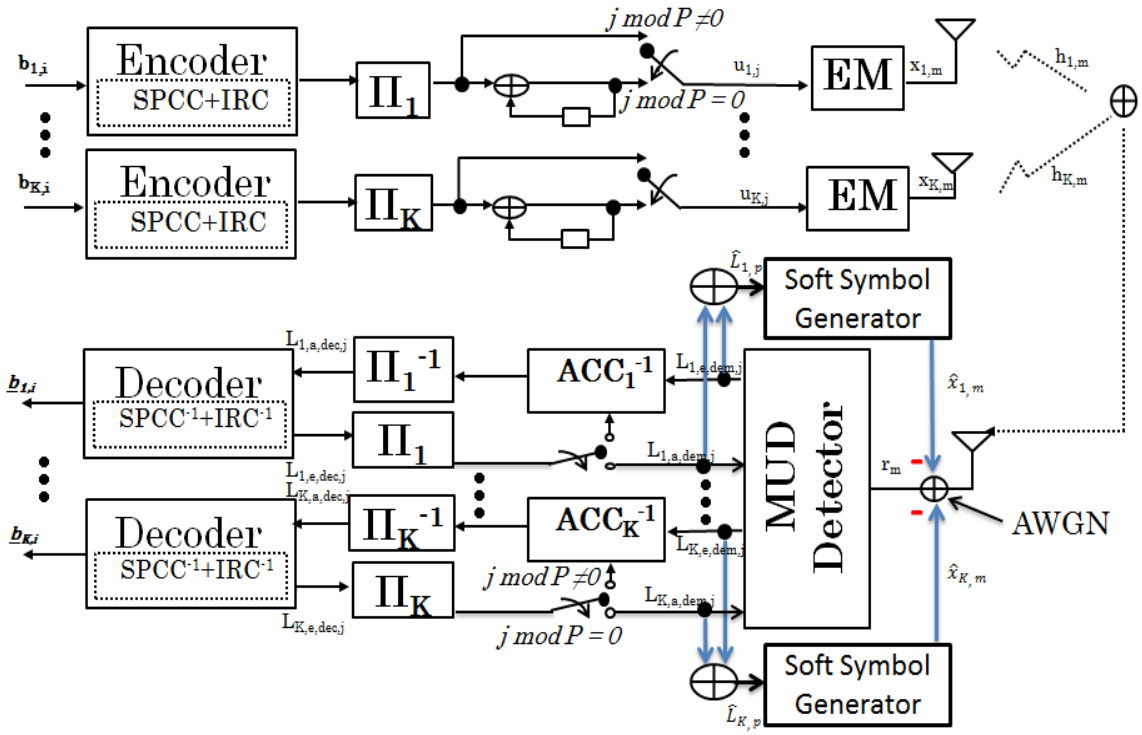

Figure 4.6: System Model of Proposed IDMA with Multiple User Detection

$$r_m = \sqrt{P_k^w} \cdot h_{k,m} \cdot x_{k,m} + \xi_{k,m} \tag{4.8}$$

with the interference from the other users plus noise

$$\xi_{k,m} = \sum_{g \neq k, g=1}^{K} \sqrt{P_g^w} \cdot h_{g,m} \cdot x_{g,m} + n_m, \tag{4.9}$$

which is consider to be the same as equation (4.4). However, since the interference from the other users are eliminated by performing soft successive interference cancellation (SSIC), the mean and variance of symbol, $E(x_{k,m})$ and $\sigma_{k,x}^2$, respectively, are updated every global iteration when the information exchange between the demapper and decoder curve in the inner loop (SUD) is finished. For the first iteration of cancellation, so-called global iteration, the mean and variance of symbol $x_{k,m}$ above are initialized, respectively, as:

$$E(x_{k,m}) = 0, \tag{4.10}$$

$$\sigma_{k,x,m}^2 = 1, \tag{4.11}$$

with the total noise variance of k^{th} user being

$$\sigma_{k,\xi,m}^2 = \sum_{g \neq k, g=1}^{K} P_g^w \sigma_{g,x,m}^2 + \sigma_n^2. \tag{4.12}$$

Substituting equation (4.12) into demapper function described above, the *extrinsic* LLRs output from demapper are computed by:

$$L_{k,e,dem}[b_{k,d}] = \ln \frac{\sum_{s \in S_0} e^{(-\frac{|r_m - s|^2}{\sigma_{k,\xi,m}^2})} \prod_{q=1, q \neq d}^{l_{map}} e^{-b_q(s) L_{k,a,dem}(b_q(s))}}{\sum_{s \in S_1} e^{(-\frac{|r_m - s|^2}{\sigma_{k,\xi,m}^2})} \prod_{q=1, q \neq d}^{l_{map}} e^{-b_q(s) L_{k,a,dem}(b_q(s))}}. \tag{4.13}$$

When more than one global iterations is performed, the mean and variance of the symbol can be updated as:

$$E(x_{k,m}) = \sum_{s \in S} s \prod_{\varpi=1}^{l_{map}} P(b_{k,\varpi} = \mp 1), \tag{4.14}$$

$$\sigma_{k,x,m}^2 = 1 - E(x_{k,m})^2 \tag{4.15}$$

with

$$P(b_{k,\varpi} = -1) = P(b_{k,\varpi} = 1) = \frac{e^{-\hat{L}_p}}{1 + e^{-\hat{L}_p}}, \tag{4.16}$$

$$P(b_{k,\varpi} = +1) = P(b_{k,\varpi} = 0) = \frac{1}{1 + e^{-\hat{L}_p}}, \tag{4.17}$$

or can be simplified as

$$P(b_{k,\varpi} = W) \quad = \quad \frac{e^{-b_{k,\varpi}\hat{L}_p}}{1 + e^{-\hat{L}_p}}, \tag{4.18}$$

where $W \in \{0, 1\}$, and $\hat{L}_p$ denotes the *a posteriori* information fed back to generate the soft symbol replica $\hat{x}_{k,m} \equiv E(x_{k,m})$, defined as:

$$\hat{L}_p = L_{k,a,dem,j} + L_{k,e,dem,j}. \tag{4.19}$$

The received signals are updated, before being fed into the demapper to estimate the *extrinsic* information for the following iteration, by subtracting the expectation values of $\xi_{k,m}$ from the original received signal, as:

$$\hat{r}_m = r_m - E(\xi_{k,m}), \tag{4.20}$$

where

$$E(\xi_{k,m}) = \sum_{g=1}^{K} h_{g,m} \cdot E(x_{g,m}) - h_{k,m} \cdot E(x_{k,m}). \tag{4.21}$$

Then, the expectation of total noise variance of k^{th} user can be computed by:

$$\hat{\sigma}^2_{k,\xi,m} \quad = \quad \sum_{g \neq k, g=1}^{K} |h_{g,m}|^2 \cdot \sigma^2_{g,x,m} + \sigma^2_n. \tag{4.22}$$

Thus, the demapper function in equation (4.13) can be rewritten as:

$$L_{k,e,dem}[b_{k,d}] = \ln \frac{\sum_{s \in S_0} e^{(-\frac{|\hat{r}_m - s|^2}{\hat{\sigma}^2_{k,\xi,m}})} \prod_{q=1, q \neq d}^{l_{map}} e^{-b_q(s) L_{k,a,dem}(b_q(s))}}{\sum_{s \in S_1} e^{(-\frac{|\hat{r}_m - s|^2}{\hat{\sigma}^2_{k,\xi,m}})} \prod_{q=1, q \neq d}^{l_{map}} e^{-b_q(s) L_{k,a,dem}(b_q(s))}}, \tag{4.23}$$

where $\hat{r}_m$ and $\hat{\sigma}_{k,\xi,m}$ are updated every global loop before providing them into the demapper. It can be seen that the cancellation process described above does not require covariance matrix inversion, and hence is more simpler than MMSE technique required for CDMA with MUD. The computational complexity is only mainly due to the demapper plus several additions/subtractions and multiplications needed for updating the mean and variance of transmitted and received signals. Therefore, the IDMA with MUD technique is more preferable than CDMA with MMSE. The simulation results of the proposed IDMA with MUD technique are provided in **Chapter 5**.

Chapter 5

Simulation Results

In this chapter, all the simulation results of the proposed techniques described in **Chapter 3** and **Chapter 4** are shown, respectively. It covers both EXIT chart analysis and BER performance. Firstly, the simulation results of SPCCIRC-BICM-ID with balanced labelling EM with modulation doping technique will be represented. After that, the results of the investigation on designing 16-QAM EM, aiming to achieve a higher spectrum efficiency, is described. Due to the shaping loss of the 16-QAM, the evaluation of both distances from the Shannon limit and coding limit are considered. Lastly, the performance analysis of IDMA for both SUD and MUD cases for a certain number of users, under AWGN channels, are provided.

5.1 Balanced Labelling EM with Modulation Doping Technique

By using the labelling mapping pattern, illustrated in Fig. 3.12 and Fig. 3.13, obtained by EBSA described in **Chapter 3**, the EXIT analysis of SPCCIRC-BICM-ID combined with MD technique are depicted in Fig. 5.1 and Fig. 5.2, respectively. It can be observed here that they are closely matched each other in the both cases, and therefore, very excellent BER performances can be expected. However, the iterations needed for demapping and decoding grows also larger due to the narrow convergence tunnel between the demapper and decoder EXIT curves. Fig. 5.3 shows the BER performance corresponding to the two EXIT curves, where parameters are given in the box under the BER chart. As can be seen that the error rates of both curves are not visible within the BER range evaluated, and the distance in SNR from the Shannon limit are only roughly 0.59 dB and 0.89 dB with the spectrum efficiency 1.05 and 1.43 bits per 4-QAM symbol, respectively. Moreover, it can be also viewed that the turbo-cliffs of both cases are very sharp because, by introducing partial accumulator, the intersection points of the demapper and decoder EXIT curves are very close to (1.0, 1.0) MI point in these cases. However, 300 iterations are needed around the turbo-cliff regions.

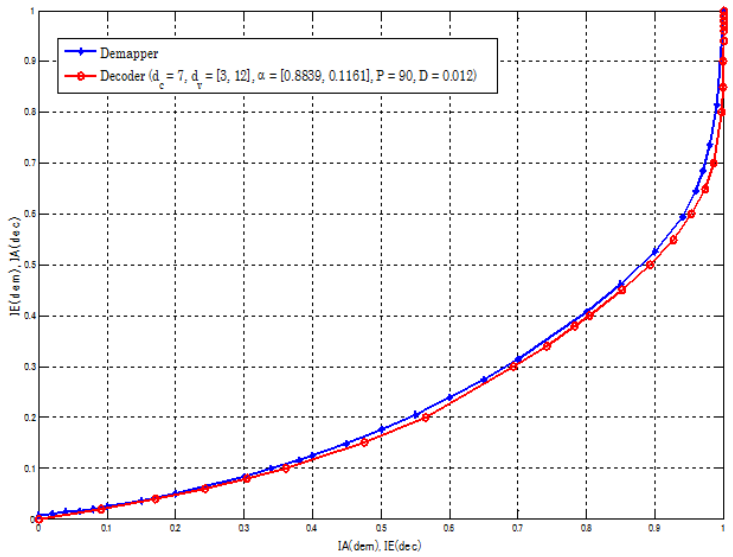

Figure 5.1: EXIT Chart of Balanced 4-QAM Extended Mapping at SNR = 0.8 dB

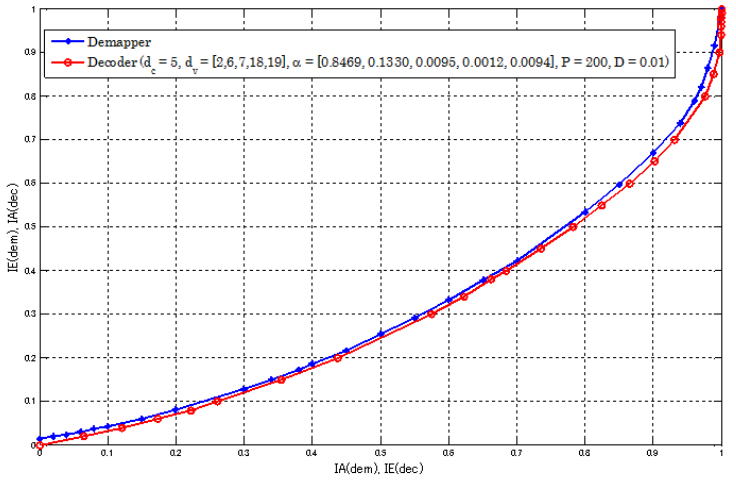

Figure 5.2: EXIT Chart of Balanced 4-QAM Extended Mapping at SNR = 3.1 dB

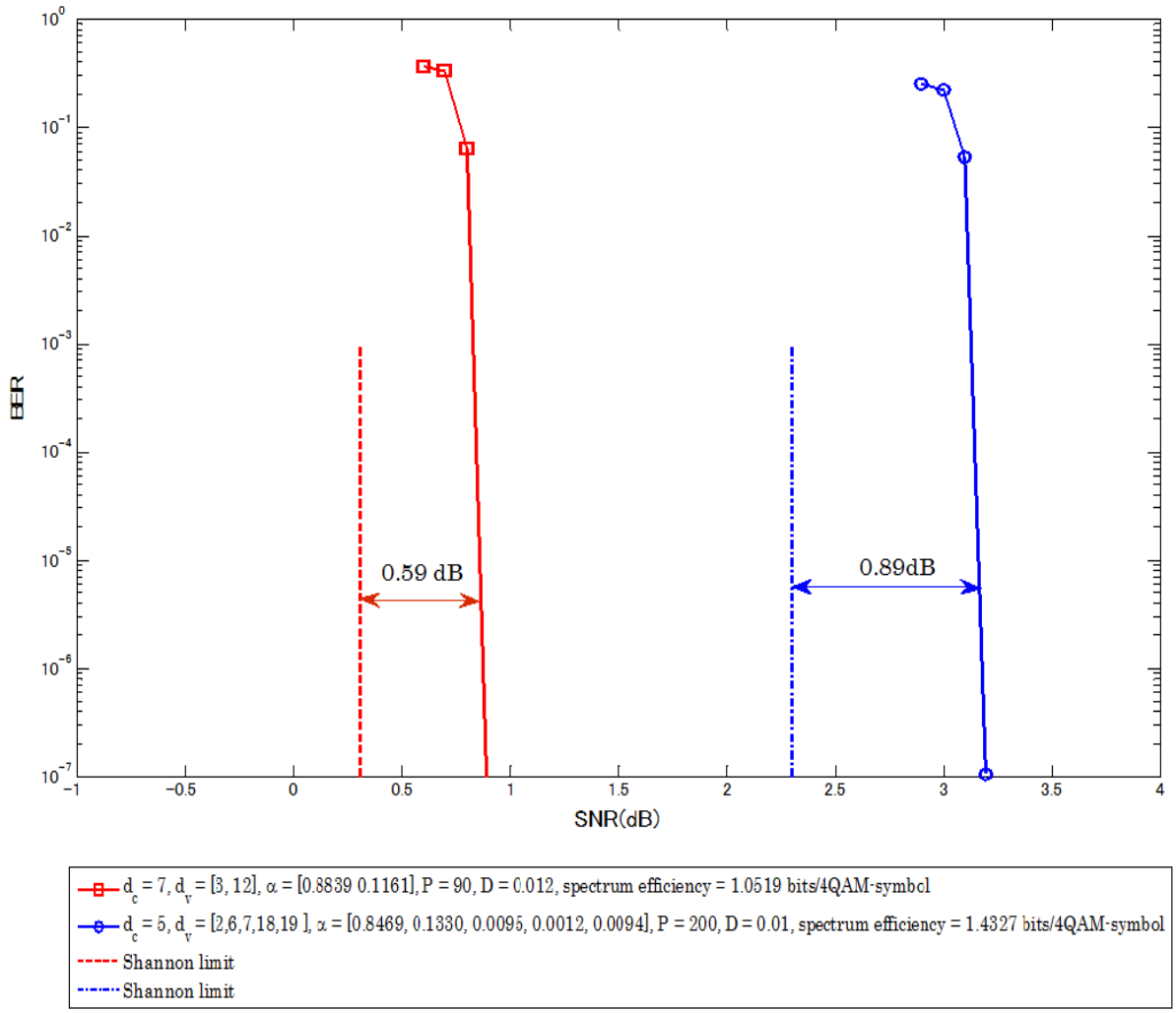

Figure 5.3: BER Chart of Balanced 4-QAM Extended Mapping

5.2 16-QAM Extended Mapping

Similarly to the case of 4-QAM based EM with MD, described above, using the labelling rules in Fig. 3.14, Fig. 3.15, and Fig. 3.16, the EXIT analysis are shown in Fig. 5.4, Fig. 5.5, and Fig. 5.6, respectively. With two bits extension of the square 16-QAM ($l_{map} = 6$), labelling pattern and the node degree allocation, were determined to achieve a higher spectrum efficiency that can not be obtained only by using 4-QAM extended mapping. Note that throughout the investigation over SPCCIRC-BICM-ID with 16-QAM EM, only a single signal constellation diagram, 16-QAM extended mapping, is adopted, since the left most part of the demapper and decoder EXIT curves do not intersect each other at very low (0.0, 0.0) MI point.

The BER performances corresponding to the three EXIT curves, mentioned above, are given in Fig. 5.7. The parameters used for the simulations, as well as the distances in decibel from the Shannon limit and CCC limit, are also denoted in the box under the BER chart. It can be observed that with the higher spectrum efficiency compared to 4-QAM, the very good BER performances are still achievable for three cases. The results show that the clear turbo-cliffs, corresponding to the threshold SNRs, are achievable at roughly only 0.24 dB, 0.30 dB, and 0.6 dB away from the 16-QAM limit with the spectrum efficiency around 1.33, 1.96 and 2.53 bits per complex dimension, respectively. It should be emphasized here that with spectrum efficiency around 1.33 bits per complex dimension seems to be quite low, however, it is difficult to achieve 1.33 bits/4-QAM spectrum efficiency only by using 4-QAM with such a good performance. In addition, since the shaping loss around the area with this low spectrum efficiency is smaller than the cases of higher spectrum efficiency, its performance outperforms the cases with higher spectrum efficiency as well. Fig. 5.8 depicts the achieved points (Eb/N0 versus spectrum efficiency) with the proposed simple BICM-ID with extended mapping, for both 4-QAM and 16-QAM, where the Gaussian capacity and CCC limit are also shown.

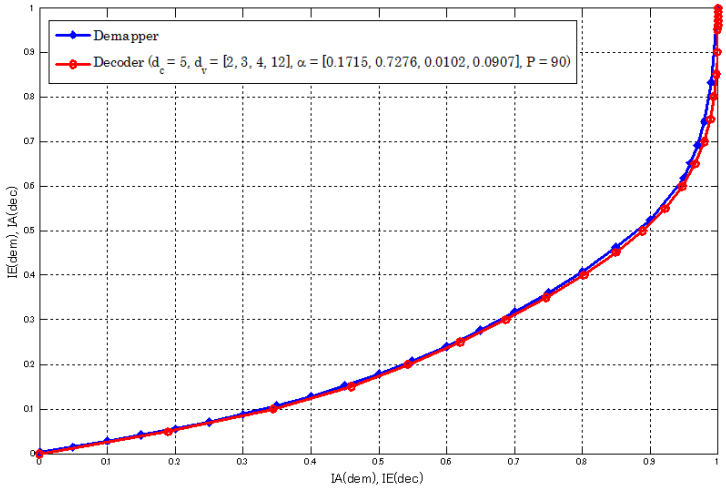

Figure 5.4: EXIT Chart of Balanced 16-QAM Extended Mapping at SNR = 2.1 dB

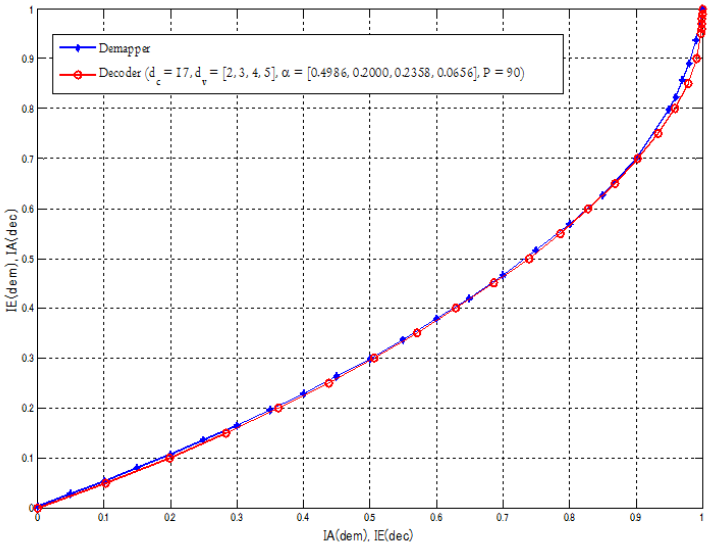

Figure 5.5: EXIT Chart of Balanced 16-QAM Extended Mapping at SNR = 5.2 dB

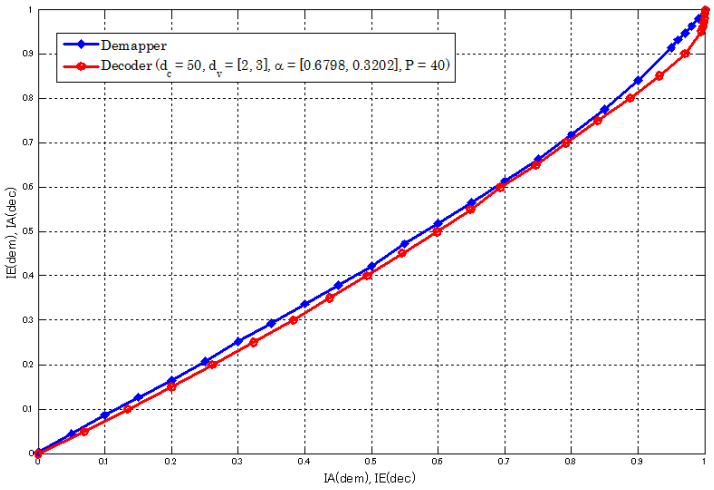

Figure 5.6: EXIT Chart of Balanced 16-QAM Extended Mapping at SNR = 8.0 dB

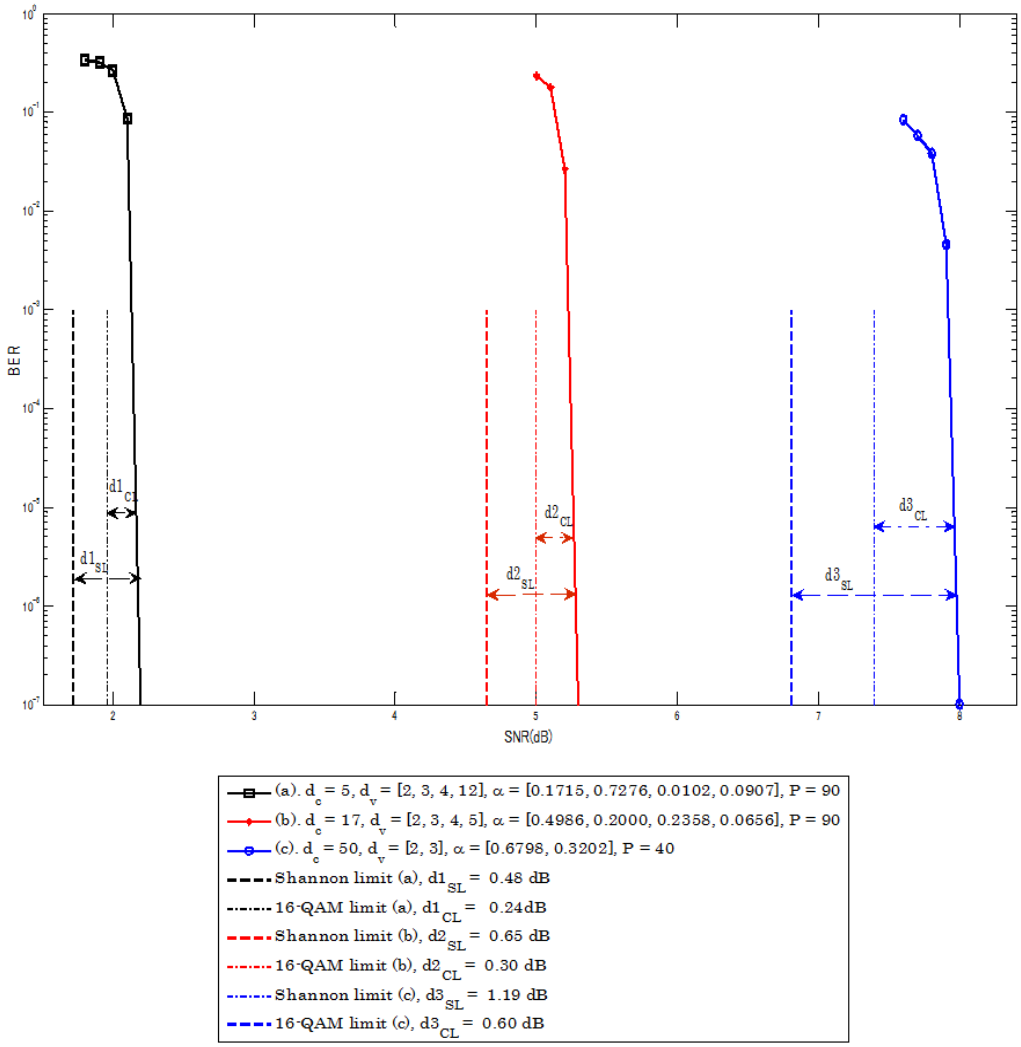

Figure 5.7: BER Chart of Balanced 16-QAM Extended Mapping

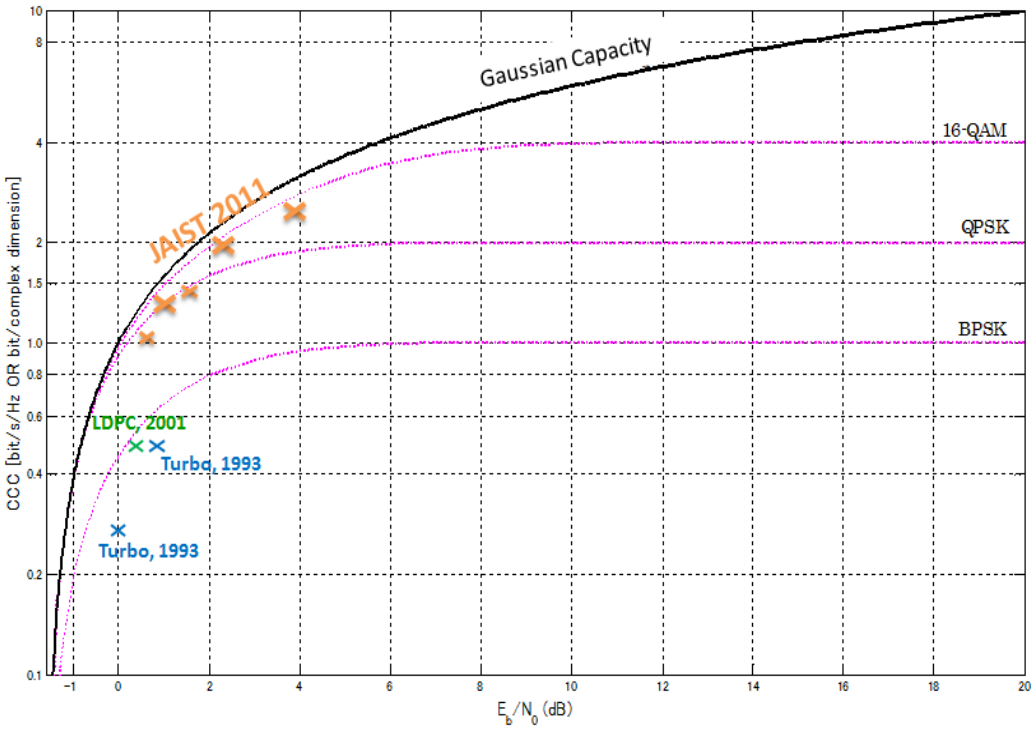

Figure 5.8: Gaussian Capacity and CCC limit

5.3 Single User Detection for BICM-ID based IDMA

Since the BICM-ID based IDMA system with SUD technique does not require successive interference cancellation, it only performs detecting and decoding, user by user, independently, without giving any *a priori* information to help other users. Therefore, the BER performance versus SNR of IDMA with SUD technique, as shown later, degrades when the number of users increases. By using labelling patterns in Fig. 4.3 and Fig. 4.4, the EXIT analysis are given as the followings. For the IDMA system evaluation, this thesis defines three different signal-noise ratios; signal-interference-plus-noise ratio (SINR), SNR for each user, and SNR for entire system. They are defined as:

$$SINR_k = \frac{P_k^w}{\sum_{g\neq k, g=1}^{K} P_g^w + \sigma_n^2}, \tag{5.1}$$

$$SNR_k = \frac{P_k^w}{\sigma_n^2}, \tag{5.2}$$

$$SNR_{system} = \frac{\sum_{k=1}^{K} P_k^w}{\sigma_n^2}, \tag{5.3}$$

where P_k^w and σ_n^2 denote the power allocated to k^{th} user and AWGN noise variance, respectively. Fig. 5.9 depicts the EXIT curve of a single user, 2 users, 5 users, and 8 users cases for SINR = -9.7 dB. It is found that, in all cases, almost the same *extrinsic* information can be achieved at the demapper output. This is because the interferer's signal point is kept the same, but the AWGN noise variance σ_n^2 decreased/increased when the number of users is increased/decreased. The BER performance is depicted in Fig. 5.11.

If the same AWGN noise variance is assumed, the degradation due to the increase in number of other interferers is analysed in Fig. 5.10. The BER performances of each user and entire system in SNR are illustrated in Fig. 5.12 and Fig. 5.13, respectively. It can be observed from Fig. 5.13 that the system error rate performance of 8 users case is worse than that of single user case, and the gap to the Shannon limit between those two curves is around 4.5 dB (= -5.59 dB - 1.03 dB).

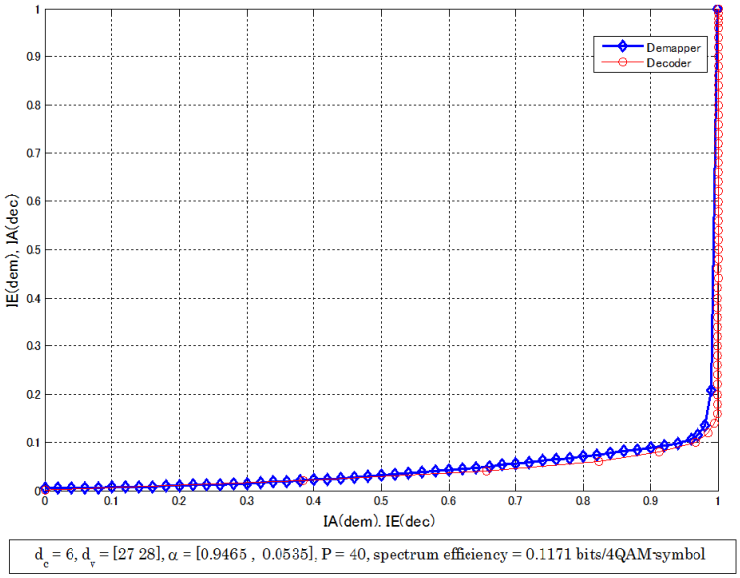

Figure 5.9: EXIT Chart of IDMA with SUD technique for 1, 2, 5, and 8 users at SINR = -9.7 dB

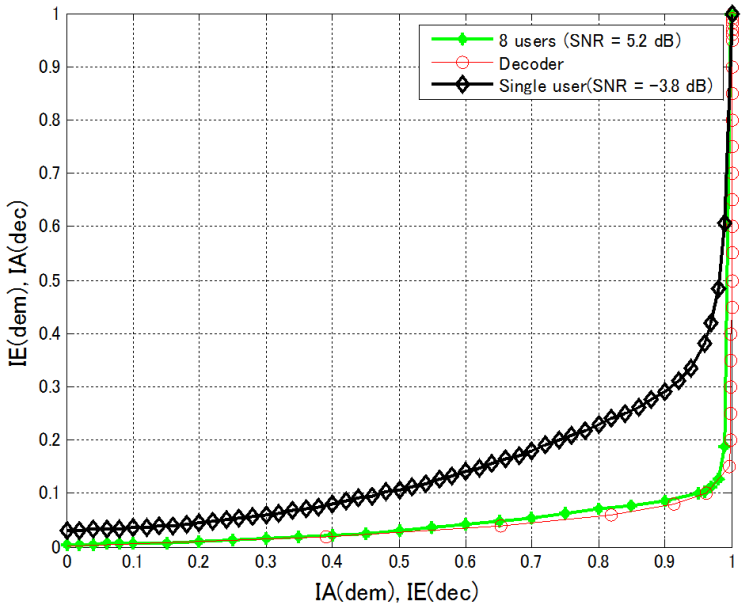

Figure 5.10: EXIT Chart of IDMA with SUD technique using the same value of σ_n^2

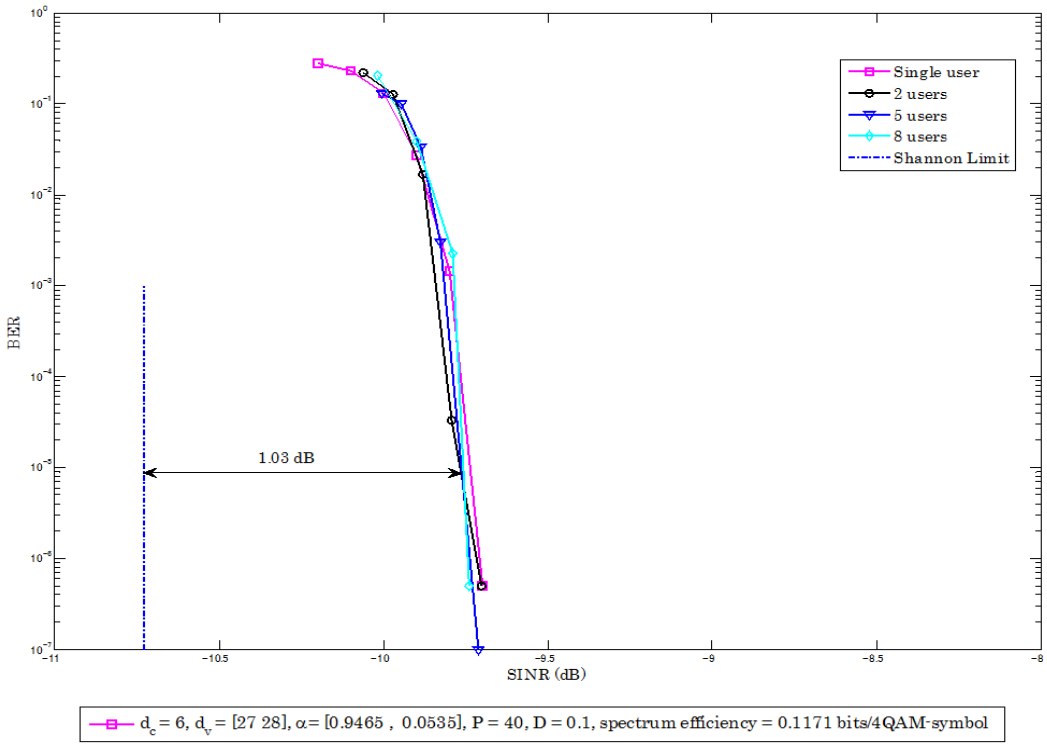

Figure 5.11: BER Chart of IDMA with SUD for Each User Evaluation in SINR with $\eta_{SPCCIRC} = 0.1171$ bits/complex dimension

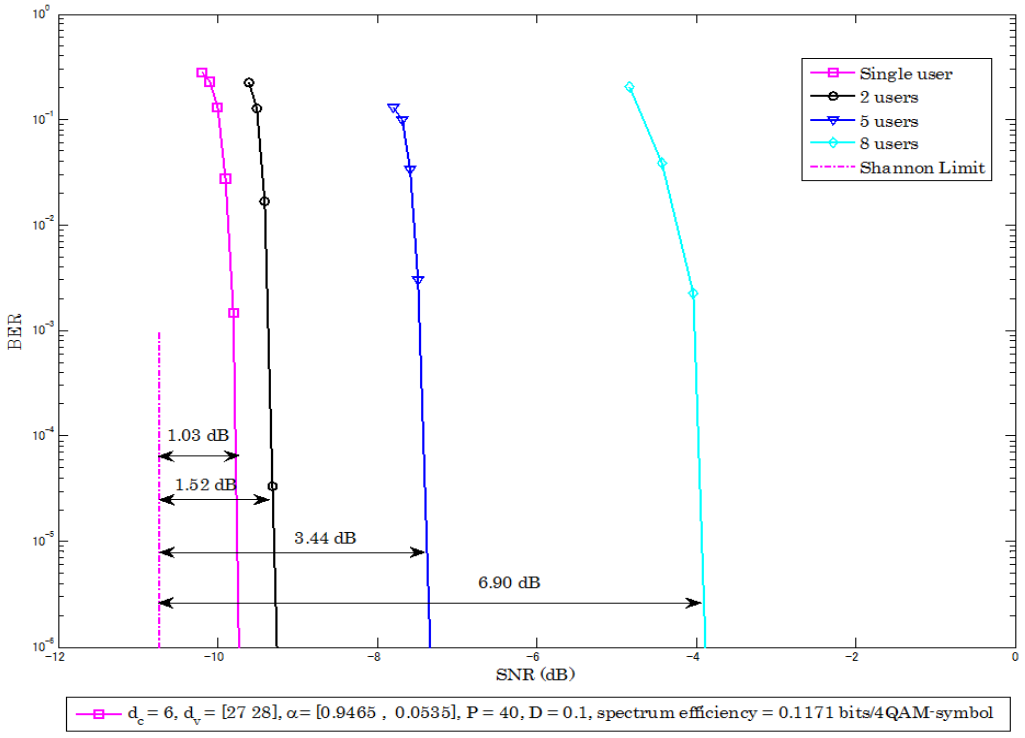

Figure 5.12: BER Chart of IDMA with SUD for Each User Evaluation with $\eta_{SPCCIRC} = 0.1171$ bits/complex dimension

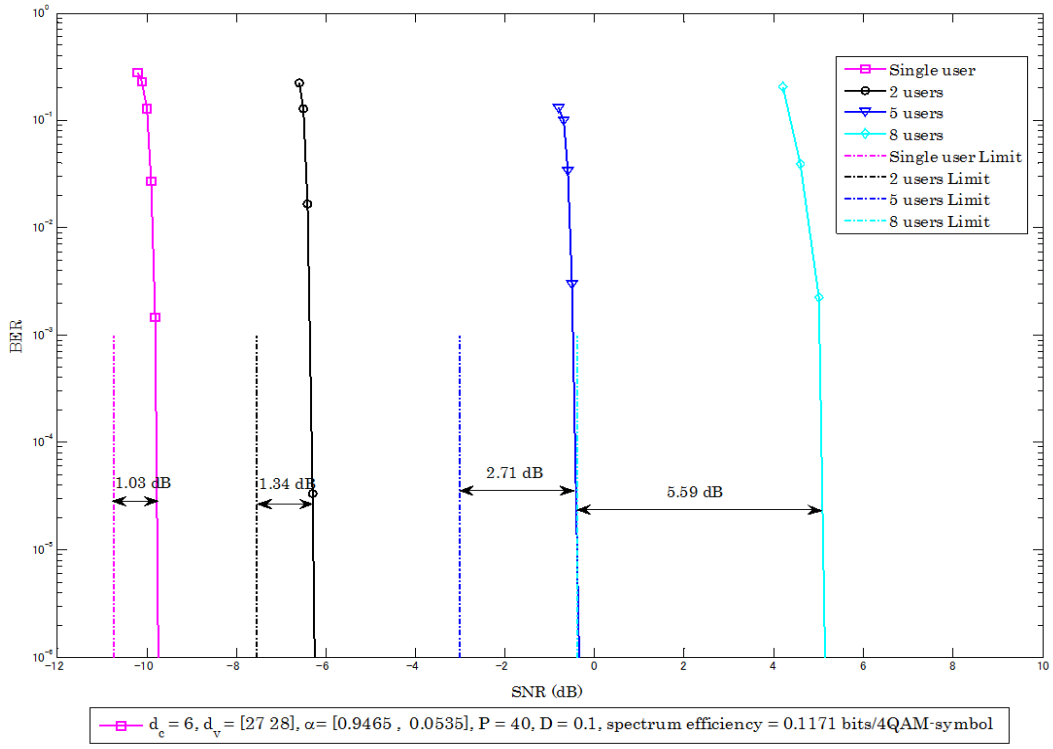

Figure 5.13: BER Chart of IDMA with SUD for Entire System Evaluation with $\eta_{SPCCIRC} = 0.1171$ bits/complex dimension

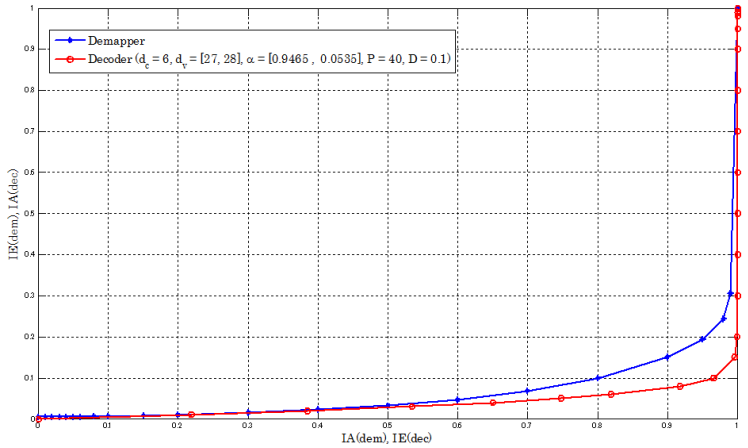

Figure 5.14: EXIT Chart of IDMA with MUD Technique at SNR = -5.6 dB

5.4 Multiple User Detection for BICM-ID based IDMA

With the BICM-ID based IDMA technique, excellent performance, in SINR, can be achieved in the case of SUD. In addition, it exhibits high information security. However, when the number of users increases, the performance degrades due to the multiple access interference from other users. Therefore, to achieve better performance, a technique to reduce or ultimately eliminate the interference, such as SSIC is needed. This thesis has proposed BICM-ID based IDMA with MUD in the previous chapter. This section provides simulation results of the proposed technique.

The simulation results are shown, as in SUD, in terms of BER versus SNR for each user and SNR for entire system. The simulation results were obtained assuming two different designs of channel coding. One is designed to achieve a good matching between the multiple users demapper EXIT curve and the decoder EXIT curves of a single user, assuming that the interference from all simultaneous users can be cancelled. The other is aimed to achieve a very small matching gap between two components' EXIT curves for multiple number of users; 8 users were assumed in the simulation. The former indicates the case where all the interference impairments from the other users can be fully cancelled by the global loop in MUD, while the later corresponds to the case where although interference can be cancelled by MUD, each user uses a code which is optimal in the multiple user scenario.

The EXIT analysis corresponding to the former case are presented in Fig. 5.14, Fig. 5.15, and Fig. 5.16. The BER performance for each user and entire system in SNRs, defined above, are shown, respectively, in Fig. 5.20 and Fig. 5.21. It can be observed that the interference from the other users can be reduced by SSIC MUD technique. The result in Fig. 5.21 shows that the threshold SNR is only roughly 3.82 dB away from the Shannon limit, where only a several global iterations were invoked. However, due to the convergence tunnel between the demaper and decoder EXIT curves remains quite large in 8 users, the

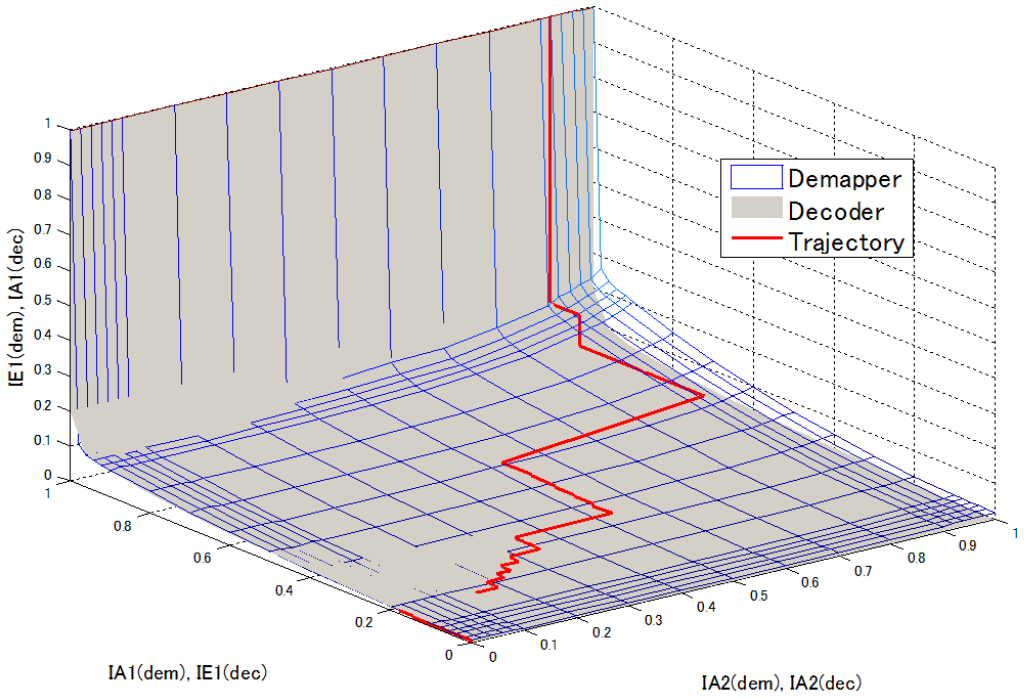

Figure 5.15: EXIT Chart of IDMA with MUD Technique at SNR = -5.6 dB in 3 Dimensions

performance is still not good enough. This is mainly because the code was designed to match with the demapper EXIT curve of a single user, not 8 users, and therefore, it is preferred that the code could be designed to achieve a close matching with the 8 users case.

The EXIT analysis of the later case, of which the aim is, as described before, to design a code which is closely matched between the demapper and decoder EXIT curves with 8 users, are drawn, in order, in Fig. 5.17, Fig. 5.18, and Fig. 5.19, with the BER performance in Fig. 5.22 and Fig. 5.23 as a proof of system evaluation. It can be seen from Fig. 5.23 that the performance is better than the former case, only roughly 1.7 dB in the threshold SNR away from the Shannon limit.

The comparison between 5 inner loops and one inner loop, both with several global iterations, is also made in this section. Fig. 5.24 shows the BER performance for each user in the case that only one inner loop and 60 global loops are adopted. It can be seen that there is no big difference, only around 0.2 dB degradation, compared with the case of that 5 inner iterations and 12 global iterations, depicted in Fig. 5.22.

The comparison between the proposed BICM-ID based IDMA and another IDMA with MUD technique [16] is drawn through Fig. 5.25 and Fig. 5.26, where Fig. 5.26 cites [16]. With almost the same spectrum efficiency, the simulation results show that the proposed IDMA with MUD technique significantly outperforms the IDMA system proposed in [16]. It is around 2.5 dB better if the comparison is in terms of the distance to the Shannon

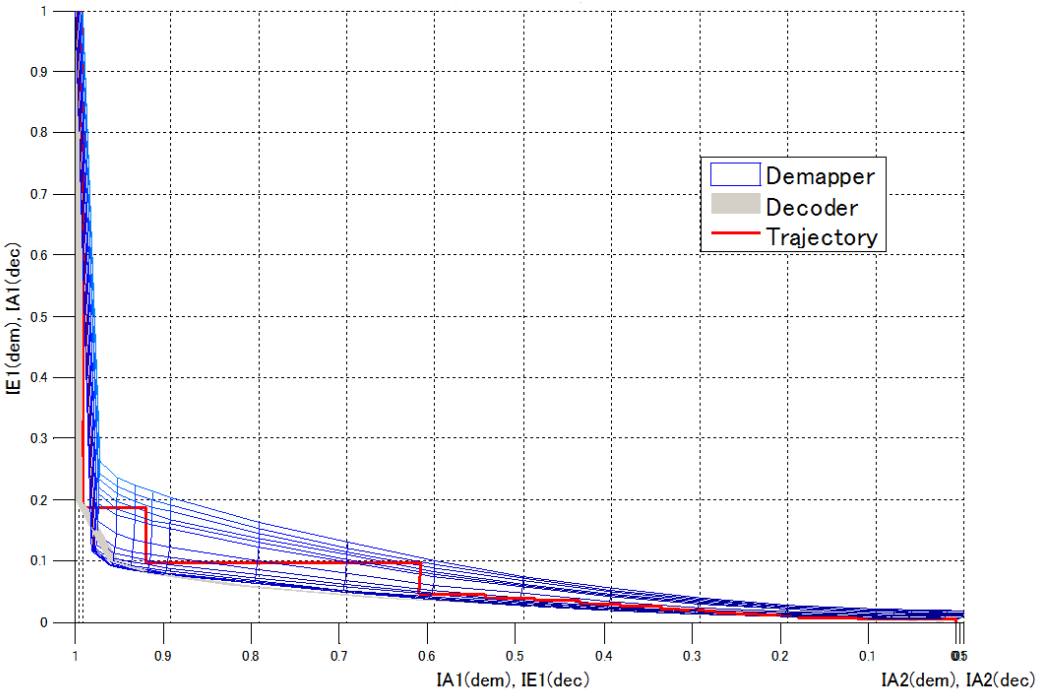

Figure 5.16: EXIT Chart of IDMA with MUD Technique at SNR = -5.6 dB with Trajectory in 2 Dimensions

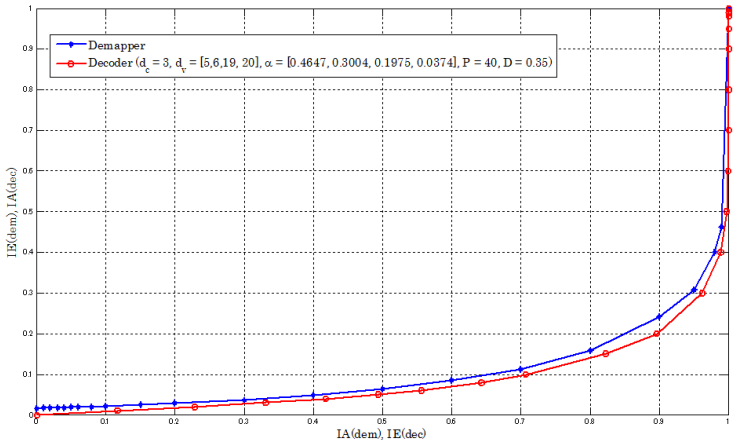

Figure 5.17: EXIT Chart of IDMA with MUD Technique at SNR = -2.4 dB

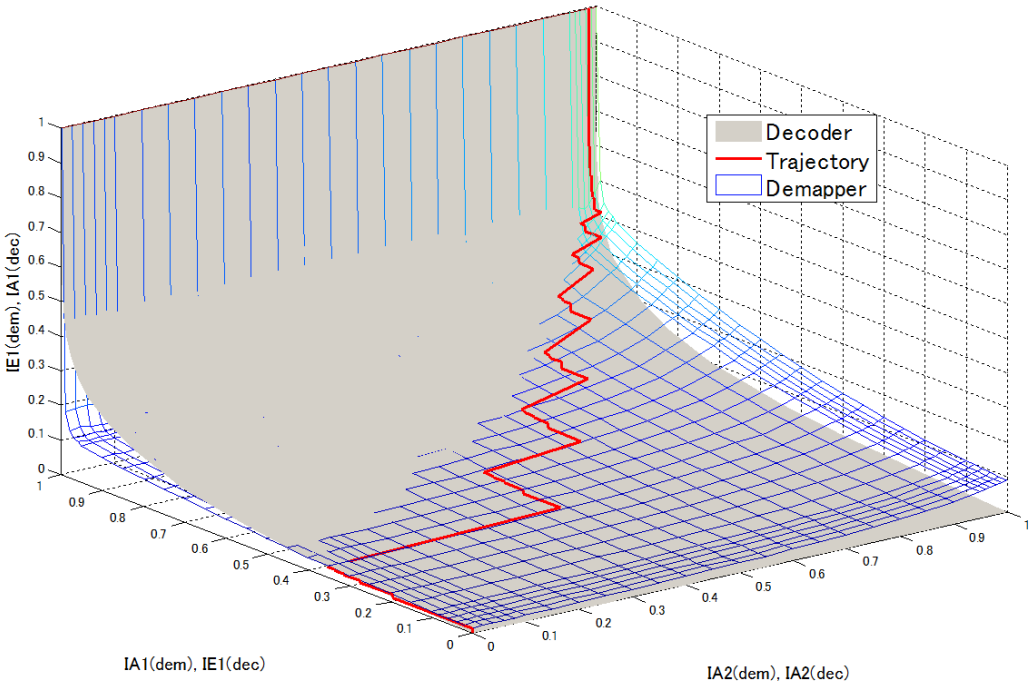

Figure 5.18: EXIT Chart of IDMA with MUD Technique at SNR = -2.4 dB in 3-D

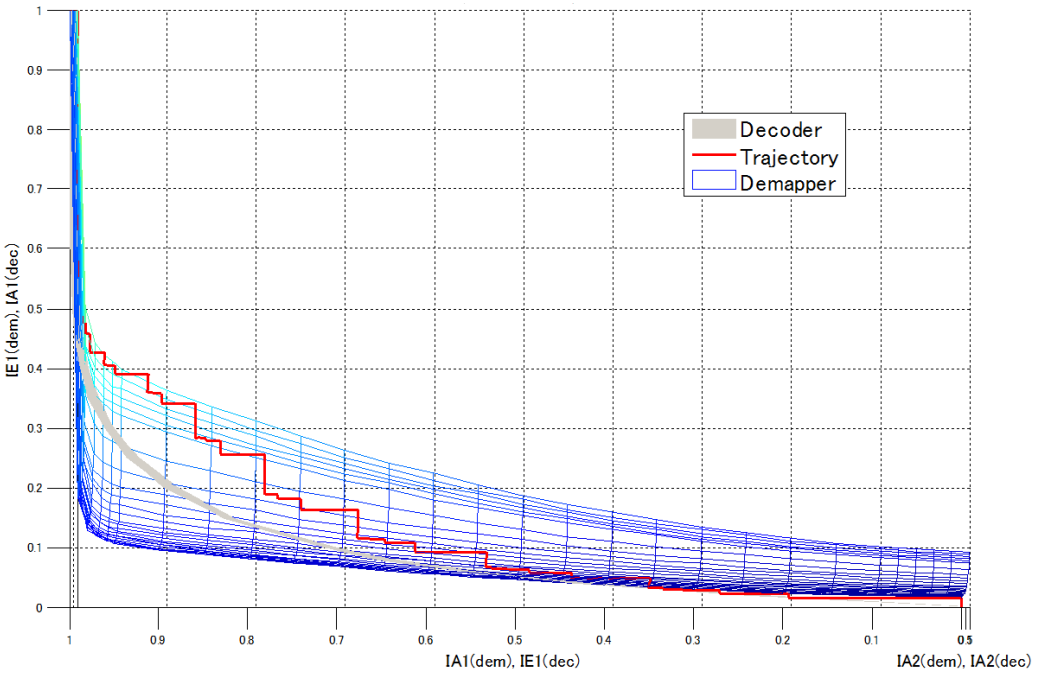

Figure 5.19: EXIT Chart of IDMA with MUD Technique at SNR = -2.4 dB with Trajectory in 2 Dimensions

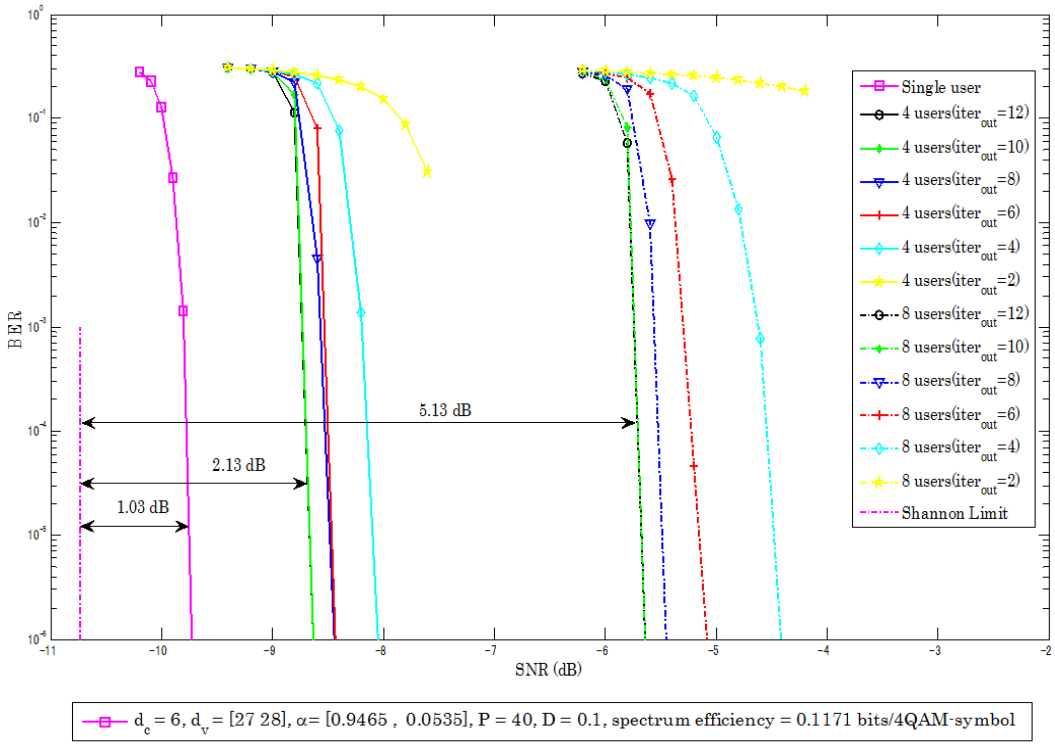

Figure 5.20: BER Chart of IDMA with MUD for Each User Evaluation with $\eta_{SPCCIRC} = 0.1171$ bits/complex dimension (inner iteration = 5)

limit.

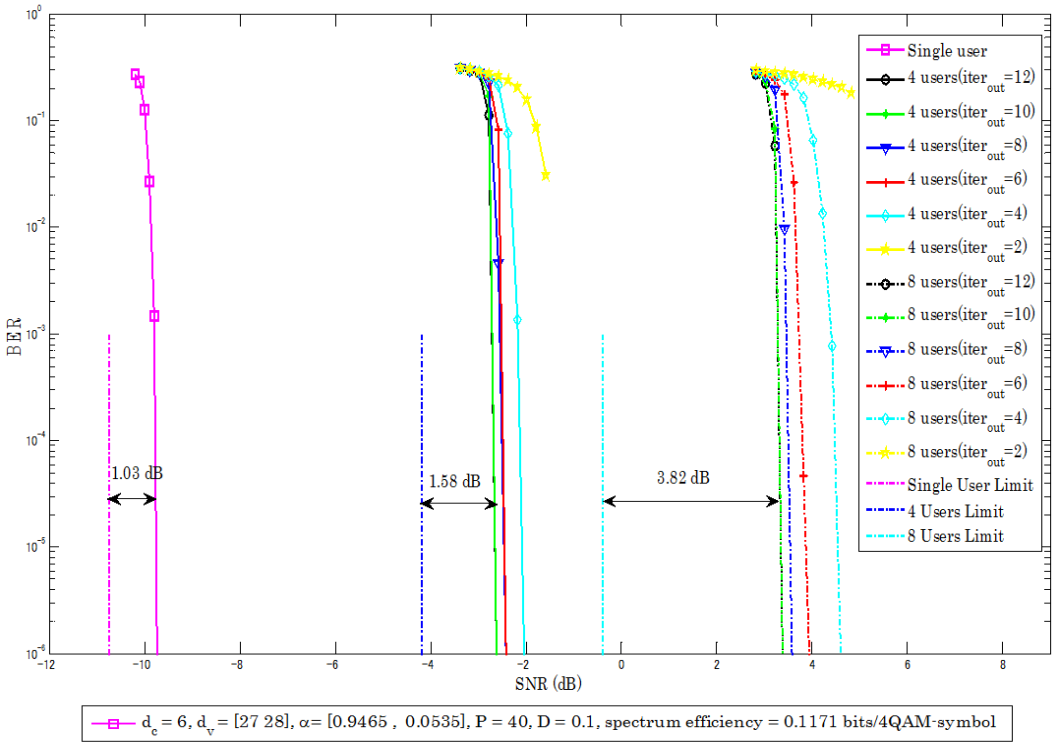

Figure 5.21: BER Chart of IDMA with MUD for Entire System Evaluation with $\eta_{SPCCIRC} = 0.1171$ bits/complex dimension (inner iteration = 5)

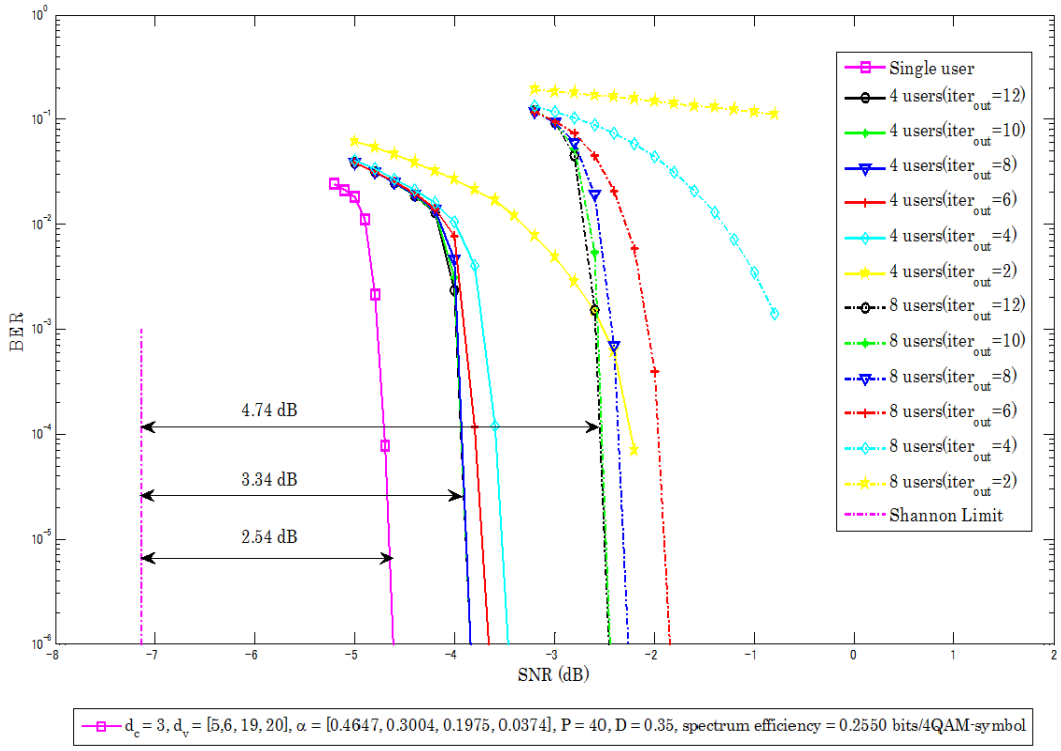

Figure 5.22: BER Chart of IDMA with MUD for Each User Evaluation with $\eta_{SPCCIRC}$ = 0.2550 bits/complex dimension (inner iteration = 5)

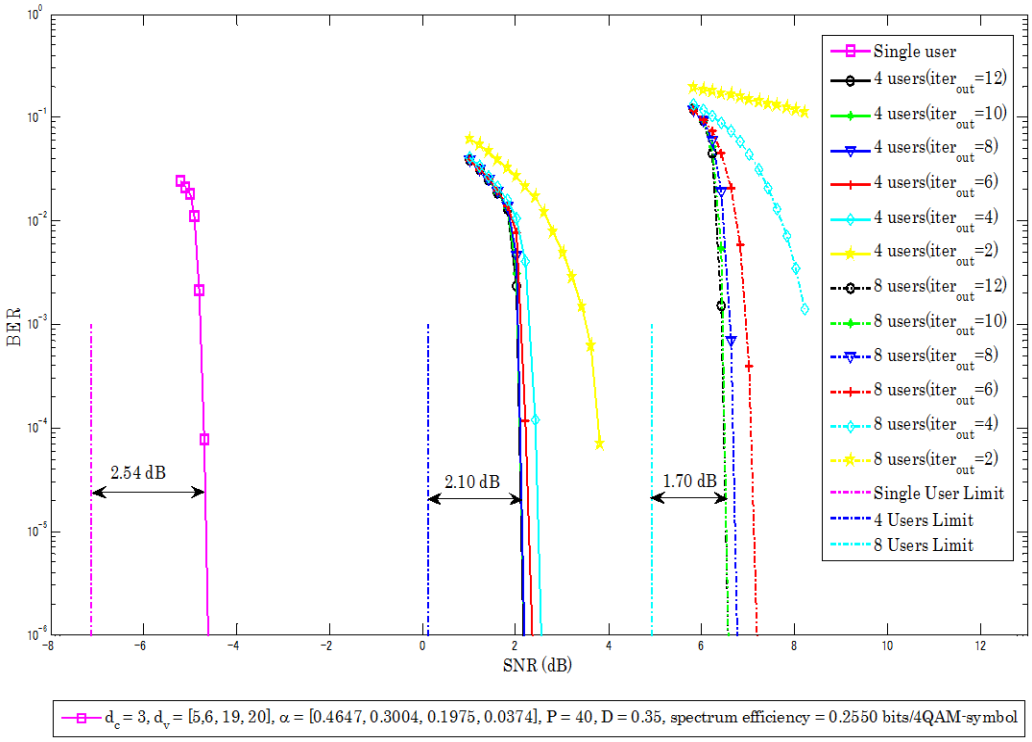

Figure 5.23: BER Chart of IDMA with MUD for Entire System Evaluation with $\eta_{SPCCIRC} = 0.2550$ bits/complex dimension (inner iteration = 5)

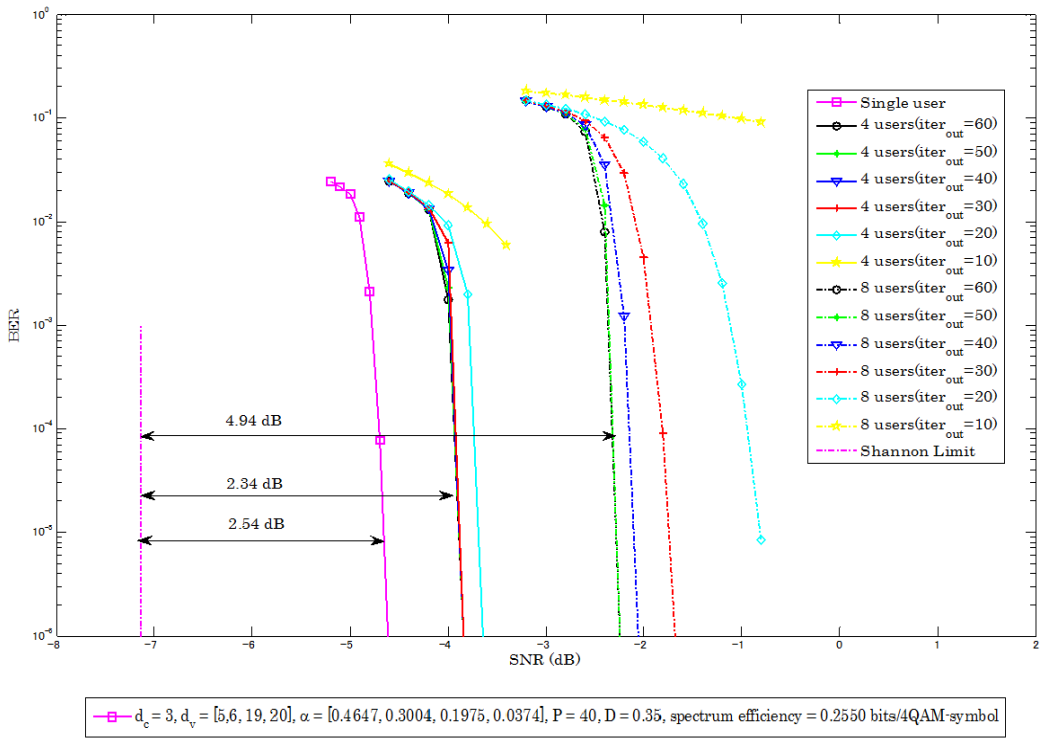

Figure 5.24: BER Chart of IDMA with MUD for Each User Evaluation with 1 Inner Loop

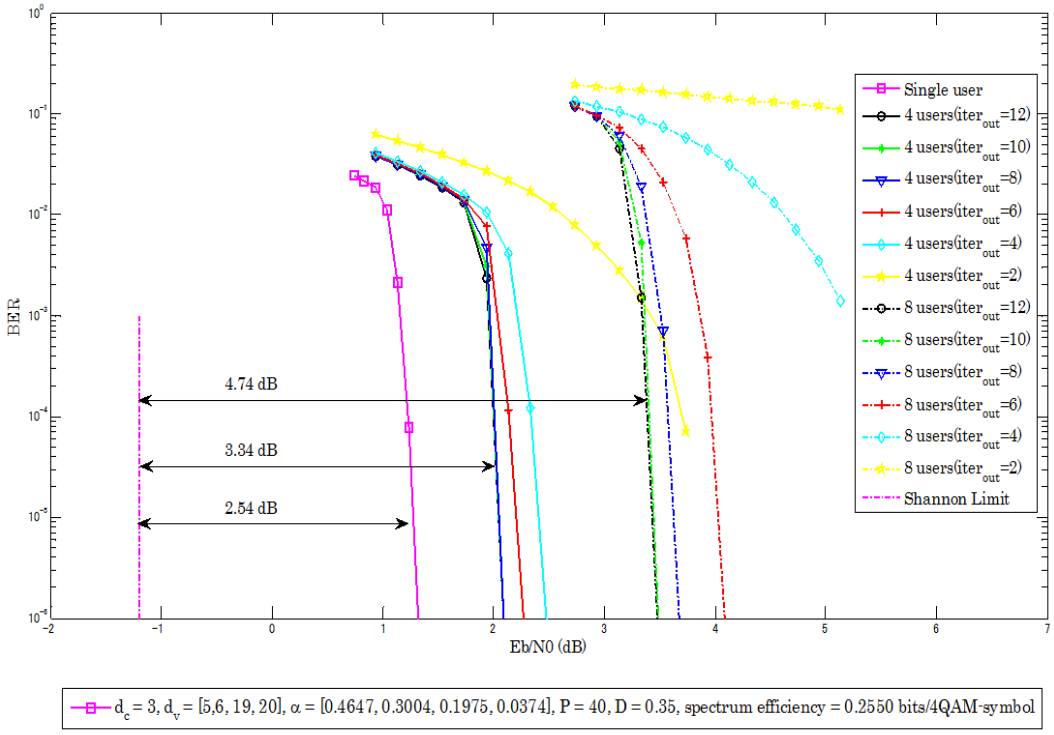

Figure 5.25: BER Chart of IDMA with MUD for Each User Evaluation in Eb/N0 with $\eta_{SPCCIRC} = 0.2550$ bits/complex dimension (inner iteration = 5)

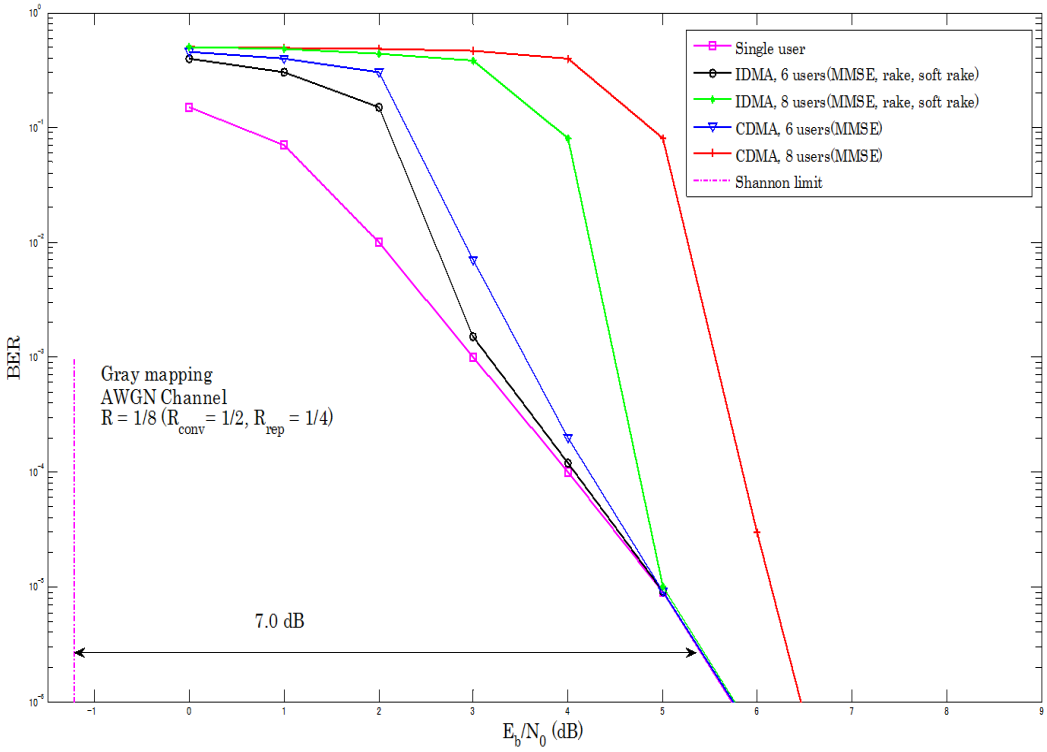

Figure 5.26: BER Chart of IDMA with MUD for Each User Evaluation in [16]

Chapter 6

Conclusions

6.1 Conclusions

This thesis has investigated two important issues, which are the designs of BICM-ID and BICM-ID based IDMA. Since the proposed technique can achieve excellent performance even though it requires only very low computational complexity, they are considered one of the most promising transmission schemes for future wireless communication systems.

In **Chapter 2**, as the tools for analysing and evaluating the system, the fundamental knowledge of EXIT and BER charts were described. It covered the knowledge about entropy, mutual information, log likelihood ratio, and J-function.

Chapter 3 mainly introduced the designs of BICM-ID for both 4-QAM and 16-QAM. It started with the proposed system model, followed by the basis of the communication channels, the joint optimization between coding and modulation using combination of BSA and LP came next, then lastly the computational complexity of the system was addressed.

In **Chapter 4**, the investigations on BICM-ID based IDMA were proposed. The system models for both SUD and MUD were first proposed. After that, the general knowledge about IDMA, including the comparison between IDMA and CDMA, the design of low rate code, as well as pros-and-cons investigations of SUD and MUD techniques were provided.

Chapter 5 provided the simulation results, EXIT Analysis and BER performance, of the entire works conducted in this research. For point to point communication, only two dimensional EXIT chart was used to design and analyze the channel coding, while for IDMA, multiple access channel transmission technique, both two and three dimension EXIT curves were adopted in order the analyse the convergence property of the code. The conclusions of the investigations on the proposed techniques, based on BER performances, are drawn as followings:

- The proposed simple BICM-ID with 4-QAM and 16-QAM extended mapping can achieve near-capacity performances, where the best results from the entire investigations are only around 0.59 and 0.48 dB away from the Shannon limit, respectively. If the distance from CCC limit of 16-QAM is considered, there is only around 0.24 dB remaining as a coding loss. The proposed system with both 4-QAM and 16-QAM,

under a certain range of SNR in AWGN channels, requires $\frac{1}{4}$ times and $\frac{1}{2}$ times, respectively, as low in computational complexity as that of the original Turbo code, introduced by C. Berrou in [2], that uses two memory-4 constituent convolutional codes.

- The results of the research on BICM-ID based IDMA with SUD technique show that it achieves excellent performance when only a single user is assumed. However, when the number of users increases larger, the performance degrades due to the interference from the other users. On the other hand, SUD technique may be a good approach if the information security is concerned. According to the proposed IDMA with MUD technique, the performance is much better than the SUD case, since the SSIC is performed with this technique. However, it is still not good enough to achieve a single user bound performance, and therefore, a new technique that may cancel all the interference from the other users is required. Even it can not achieve a single user bound, the proposed technique outperforms another technique proposed in [16]. The simulation results show that it is around 2.5 dB better if compared with the distance from the Shannon limit.

6.2 Future Challenges

This thesis has focused on three concepts for the investigations; simple system models, low computational complexity, and near-capacity-achieving (maximizing the power efficiency). It was started with a point to point communication scheme, and followed by the multiple access channel communication systems. Since almost everything has been done in the point to point communication, the next interesting steps should include multiple access channel communication, as well as its combination with the multiple relays network schemes. The future provision may be summarized in the following:

- Since the results of the SSIC of the proposed IDMA with MUD technique can not achieve a single user bound, to achieve a better performance, a new technique that may remove completely all interference, while remaining as low computational complexity as possible, is strongly required. The hybrid MUD technique, which can be seen as the combination between the proposed MUD technique and MMSE based MUD, may be one of the good choices.

- Recently, relay networks have been widely discussed due to their remarkable capability and flexibility to improve the reliable transmission among multiple users in the frequency selective fading channel. Since IDMA has advantage of being robust against the fading channels with low computational complexity, it can be used to differentiate the signals of a certain user without any synchronizations with the other nodes in relay networks. Therefore, it is a reasonable to extend the proposed BICM-ID based IDMA to the relay networks system. In addition, since the performance of the relay networks systems depends strongly on the cooperation protocols as well as the distance between (1) source and relay, along with (2) relay and destination, the idea of the adaptive distance-and-protocol cooperation relay networks is, indeed, a very interesting topic.

Appendix A: Labelling Mapping

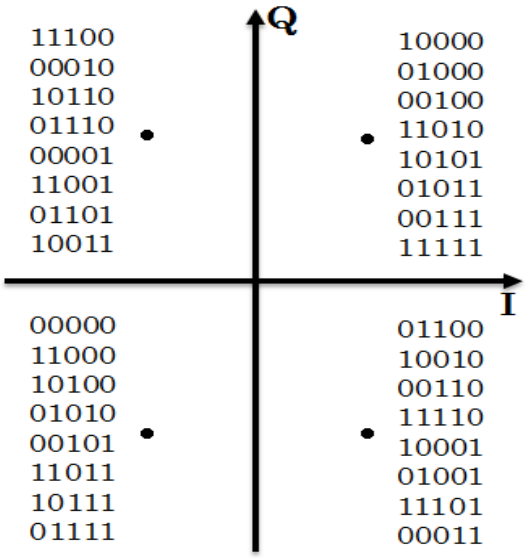

Figure 6.1: Balanced 4-QAM Extended Mapping Optimized at SNR = 0.8

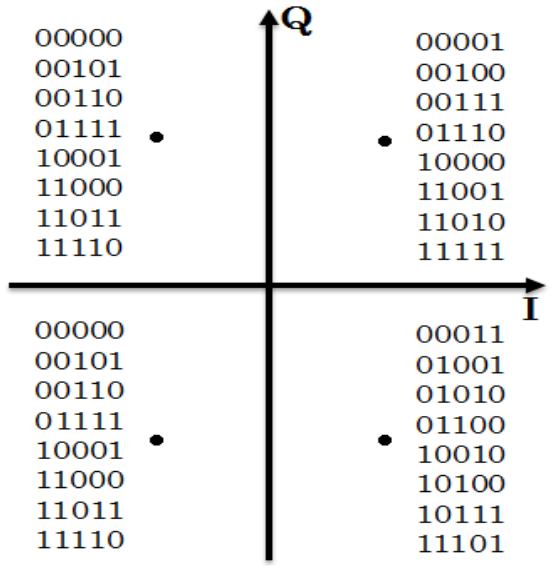

Figure 6.2: Balanced 4-QAM Extended Mapping Optimized at SNR = 3.1

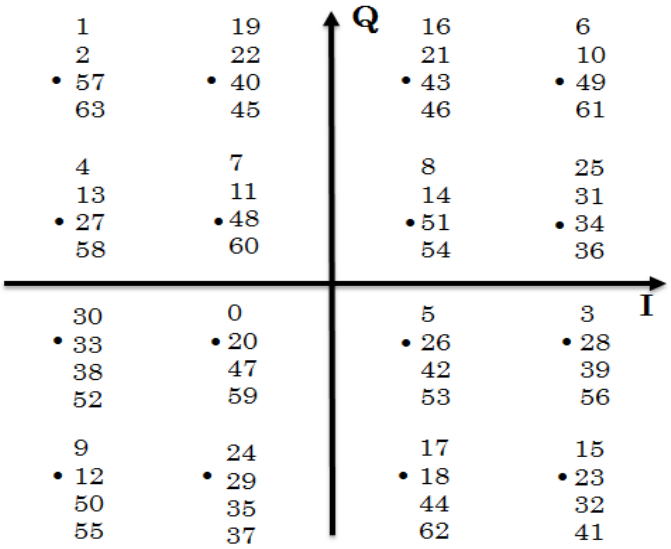

Figure 6.3: Balanced 16-QAM Extended Mapping Optimized at SNR = 2.0

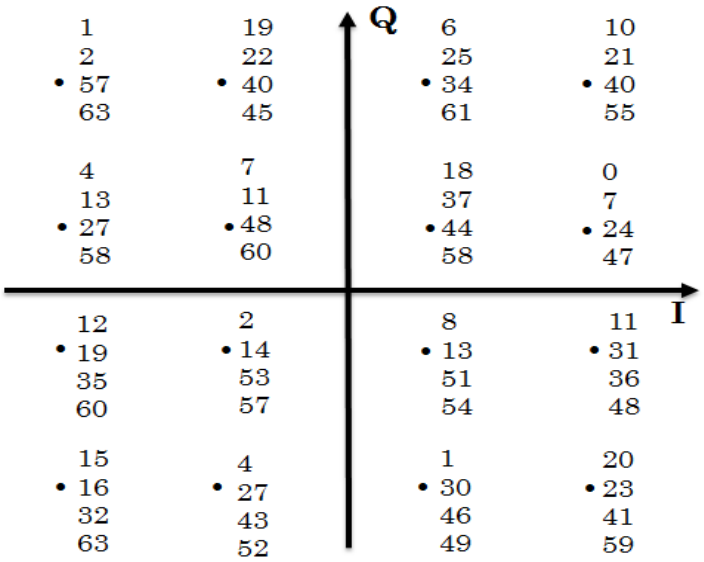

Figure 6.4: Balanced 16-QAM Extended Mapping Optimized at SNR = 5.0

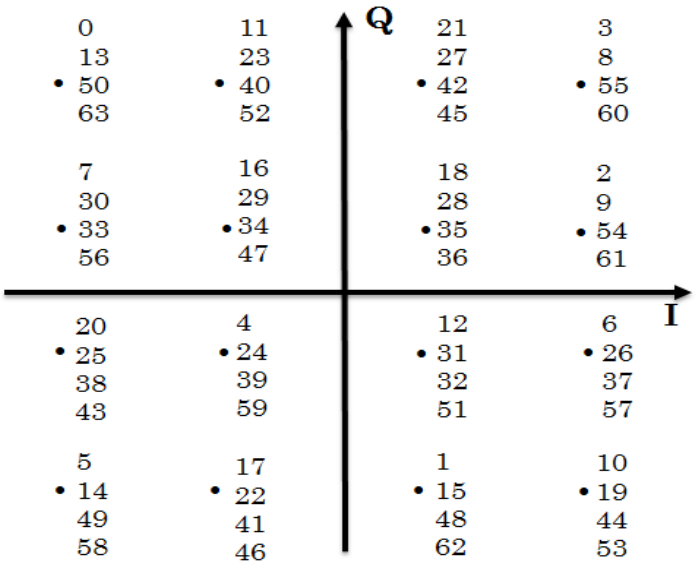

Figure 6.5: Balanced 16-QAM Extended Mapping Optimized at SNR = 8.0

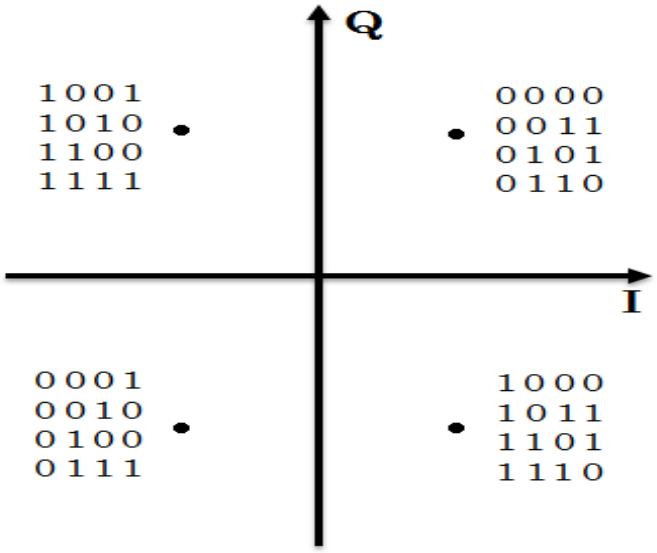

Figure 6.6: 4-QAM Extended Mapping with $l_{map} = 4$

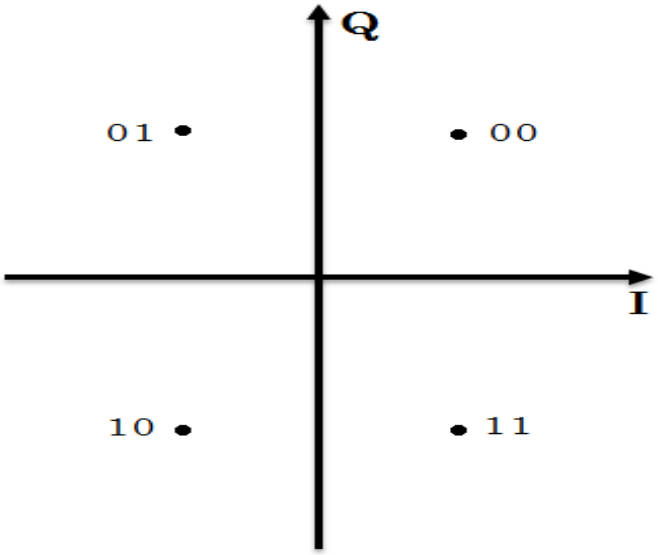

Figure 6.7: 4-QAM Standard Non-Gray Mapping with $l_{map} = 2$

Bibliography

[1] C. E. Shannon, "A mathematical theory of communication," *Bell Systems Technical Journal*, vol. 27, pp. 379-423,623-656, 1948.

[2] C. Berrou and A. Glavieux, "Near optimum error correcting coding and decoding: turbo-codes," *Communications, IEEE Transactions on*, vol. 44, no. 10, pp. 1261-1271, Oct. 1996.

[3] S. ten Brink, "Convergence Behaviour of Iteratively Decoded Parallel Concatenated Codes",*IEEE Transactions on Communications*, vol. 49, no. 10, pp. 1727-1737, 2001

[4] J. Hagenauer, "The EXIT Chart - introduction to extrinsic information transfer in iterative processing", *12th European Signal Processing Conference (EUSIPCO)*, pp. 1541-1548, 2004.

[5] E. Cela, "The Quadratic Assignment Problem", *Kluwer Academics, Norwell*, MA, 1998.

[6] R. Battiti and G. Tecchiolli, "The reactive tabu search", *ORSA Journal on Computing*, pp. 126-140, 1994.

[7] K. Zeger and A. Gersho, "Pseudo-Gray coding", *IEEE Transactions on Communications*, vol. 38, pp. 2147-2158, Dec. 1990.

[8] J. Hagenauer, E. Offer, L. Papke, "Iterative decoding of binary block and convolutional codes", *IEEE Trans. on Inform. Theory*, vol. 42, pp.429-445, Mar. 1996.

[9] L. Bahl, J. Cocke, F. Jelinek, and J.Raviv, "Optimal Decoding of Linear Codes for minimizing symbol error rate", *IEEE Transactions on Information Theory*, vol. IT-20(2), pp.284-287, Mar. 1974.

[10] S. Pfletschinger and F. Sanzi, "Error floor removal for bit-interleaved coded modulation with iterative detection", *Wireless Communications, IEEE Transactions*, vol. 5, no. 11, pp. 3174-3181, 2006.

[11] F. Schreckenbach , G. Bauch, "Irregular signal constellations, mappings and precoder", *In International Symposium on Information Theory and its Applications (ISITA)* , 2004.

[12] S. Lin and D. J. Costello, *Error Control Coding, Second Edition*. Upper Saddle River, NJ, USA: Prentice-Hall, Inc., 2004.

[13] L. Hanzo, T. H. Liew, and B. L. Yeap, *Turbo Coding, Turbo Equalisation and Space-Time Coding for Transmission over Fading Channels*. New York, NY, USA: John Wiley & Sons, Inc., 2002.

[14] P. Robertson, E. Villebrun, and P. Hoeher, "A comparison of optimal and sub-optimal M MAP decoding algorithms operating in the log domain", in *Communications, 1995. ICC '95 Seattle, 'Gateway to Globalization', 1995 IEEE International Conference on*, vol.2, Jun 1995, pp. 1009-1013.

[15] S. ten Brink, "Rate one-half code for approaching the Shannon limit by 0.1 dB," Electronics Letters, vol. 36, no. 15, pp. 1293?1294, Jul. 2000.

[16] K. Kusume, G. Bauch, W. Utschick, "IDMA Vs. CDMA: Detectors, Performance and Complexity", *Global Telecommunications Conference*, 2009. GLOBECOM 2009.

[17] P. Henkel, "Extended Mappings for Bit-Interleaved Coded Modulation", *IEEE PIMRC* 2006.

[18] L. Ping, L. Liu, K. Wu, and W. K. Leung, "Interleave-division multiple-access," IEEE Transactions on Wireless Communications, vol. 5, no. 4, pp. 938-947, April 2006.

Index